

Silicic Fe-Ti-oxide series of slow-spreading ridges: petrology, geochemistry, and genesis with reference to the Sierra Leone segment of the Mid-Atlantic Ridge axial zone at 6°N

E. V. Sharkov¹, N. S. Bortnikov¹, T. F. Zinger², and A. V. Chistyakov¹

Received 15 December 2004; revised 10 February 2005; accepted 1 March 2005; published 14 August 2005.

[1] Silicic Fe-Ti-oxide magmatic series was first recognized in the Sierra Leone axial segment of the MAR near 6°N. The series consists of intrusive rocks (harzburgites, lherzolites, bronzitites, norites, gabbronorites, hornblende Fe-Ti-oxide gabbronorites and gabbronorite-diorites, quartz diorites, and trondhjemitites) and their subvolcanic (ilmenite-hornblende dolerites) and, possibly, volcanic analogues (ilmenite-bearing basalts). The deficit of most incompatible elements in the rocks of the series suggests that the parental melts were derived from a source that had already been melted. Correspondingly, these melts could not be MORB derivatives. The origin of the series is thought to be related to the melting of the hydrated oceanic lithosphere during the emplacement of an asthenospheric plume (protuberance on the surface of a large asthenospheric lens beneath MAR). The genesis of different melts was supposedly controlled by the ascent of a chamber of hot mantle magmas thought this lithosphere in compliance with the zone melting mechanism. The melt acquired fluid components from the heated rocks at the peripheries of the plume and became enriched in Fe, Ti, Pb, Cu, Zn, and other components mobile in fluids. *INDEX TERMS*: 1032 Geochemistry: Mid-oceanic ridge processes; 1037 Geochemistry: Magma genesis and partial melting; 1065 Geochemistry: Major and trace element geochemistry; 3619 Mineralogy and Petrology: Magma genesis and partial melting; *KEYWORDS*: Slow-spreading ridges, Ultramafic cumulates, Fe-Ti-oxides.

Citation: Sharkov, E. V., N. S. Bortnikov, T. F. Zinger, and A. V. Chistyakov (2005), Silicic Fe-Ti-oxide series of slow-spreading ridges: petrology, geochemistry, and genesis with reference to the Sierra Leone segment of the Mid-Atlantic Ridge axial zone at 6°N, *Russ. J. Earth. Sci.*, 7, ES4001, doi:10.2205/2005ES000181.

Introduction

[2] The third crustal layer in slow-spreading ridges, such as the Mid-Atlantic Ridge (MAR) and the Southwest Indian Ridge, is known to consist of a broad spectrum of plutonic rocks, which include, along with primitive magnesian troctolites and gabbro, also ferrogabbro (Fe-Ti-oxide gabbro) and closely associated with it norites, gabbronorites, hornblende gabbronorites, and gabbronorite-diorites, quartz diorite, as well as veins and small bodies of plagiogranites (trondhjemitites) [Dick *et al.*, 2000; Ozawa *et al.*, 1991; Pearce, 2002; Silantyev, 1998].

[3] These rocks are still studied relatively poorly because they are commonly regarded as late derivatives of tholeiitic basalts in mid-oceanic ridges (MORB) [Dick *et al.*, 1992; Silantyev *et al.*, 1998]. However, Simonov *et al.* [1999] were the first to note that the parental melts of the Fe-Ti-oxide gabbroids could not be derivatives of either N-MORB or E-MORB, because they are oversaturated with TiO₂. These rocks are sometimes regarded even as evidence of the existence of anomalous mantle sources [Cannat *et al.*, 1992]. The nature of the trondhjemitites is also uncertain: according to Dick *et al.* [1991], these rocks were generated by the fractional crystallization or anatexis of the host amphibolized gabbroids, whereas Silantyev [1998] believes that they had had a separate deep source with anomalous geochemical characteristics typical of source like E-MORB.

[4] Our petrological and geochemical data obtained on these rocks from the Sierra Leone MAR segment indicate that these rocks display some unusual features which have not been adequately fully highlighted before. First of all, these rocks are characterized by low contents of incompatible elements, including LREE, which suggests that the parental

¹Institute of the Geology of Ore Deposits, Petrography, Mineralogy, and Geochemistry (IGEM), Russian Academy of Sciences, Moscow, Russia

²Institute of Precambrian Geology and Geochronology, Russian Academy of Sciences, St. Petersburg, Russia

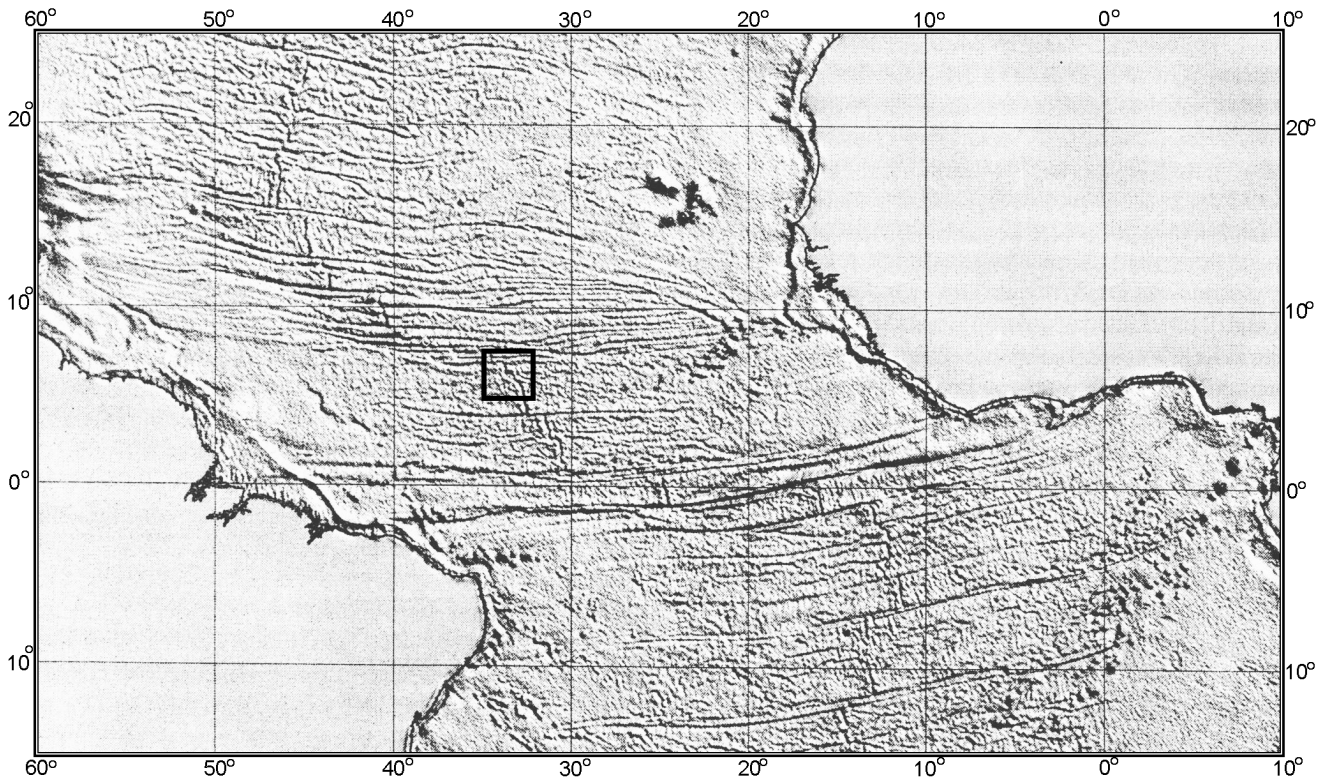


Figure 1. Location map of the study area (black square) among seafloor structures in the Central Atlantic (based on the data of satellite altimetry from [Sandwell and Smith, 1997]).

melts of these rocks were derived from sources that had already been remelted, and, thus, these rocks could hardly be MORB derivatives. Moreover, these melts exhibit some extraordinary compositional features: on the one hand, they were saturated or even oversaturated with silica and had high water contents, as is typical of magmas of the supra-subduction calc-alkaline series, and, on the other hand, were rich in Fe, Ti, and Nb, as is characteristic of within-plate (plume-related) magmas.

[5] All of these features seem to suggest that slow-spreading ridges contain, along with MORB (which are typical of such environments) and their derivatives, also an unusual type of magmatic melts, which are enriched in silica and do not fall into any of the currently adopted systematics for magmatic. This publication is devoted to the petrological-geochemical characterization of these rocks and their genesis.

Geological Overview

[6] The axial MAR segment described in this paper lies between the Bogdanov Fracture Zone (7°10' N) and 5°00' N [Pushcharovskii *et al.*, 2002; Skolotnev *et al.*, 2003a], near the Sierra Leone Fracture Zone (Figure 1). The local seafloor

has a highly dissected topography, which is characterized by the absence of transform faults and the variable strike of the rift valley, which consists here of graben-shaped depressions up to 4–5 km deep, such as the Markov depression (Figure 2). This MAR segment also differs from adjacent areas in having lower seismicity.

[7] The results of dredging during Cruise 10 of the R/V Akademik Ioffe in 2001–2002 and Cruise 22 of the R/V Professor Logachev in 2003 suggest that long (>300 km) segments of both walls of the rift valley consist of plutonic rocks, including serpentinized peridotites, various gabbroids, cataclasites and mylonites developing after mafic and ultramafic rocks, and various metasomatic rocks. Strongly altered and tectonized basalts and dolerites crop out in the floor of the valley, its northern and southern flanks, and in the upper parts of its walls. Fresh basalts with crusts of volcanic glass were found on valley floor and on the slopes of neovolcanic rises.

[8] In spite of the uneven character of the sampling, it can be definitely concluded that both walls of the valley contain similar rock complexes that characterize the whole sequence of the oceanic crust. Judging from the results of remote sensing (conducted with the use of a MAK marine acoustic complex during Cruise 22 of the R/V Professor Logachev in 2003), the local crust is clearly layered. This suggests that most of the rocks discussed in this paper compose a

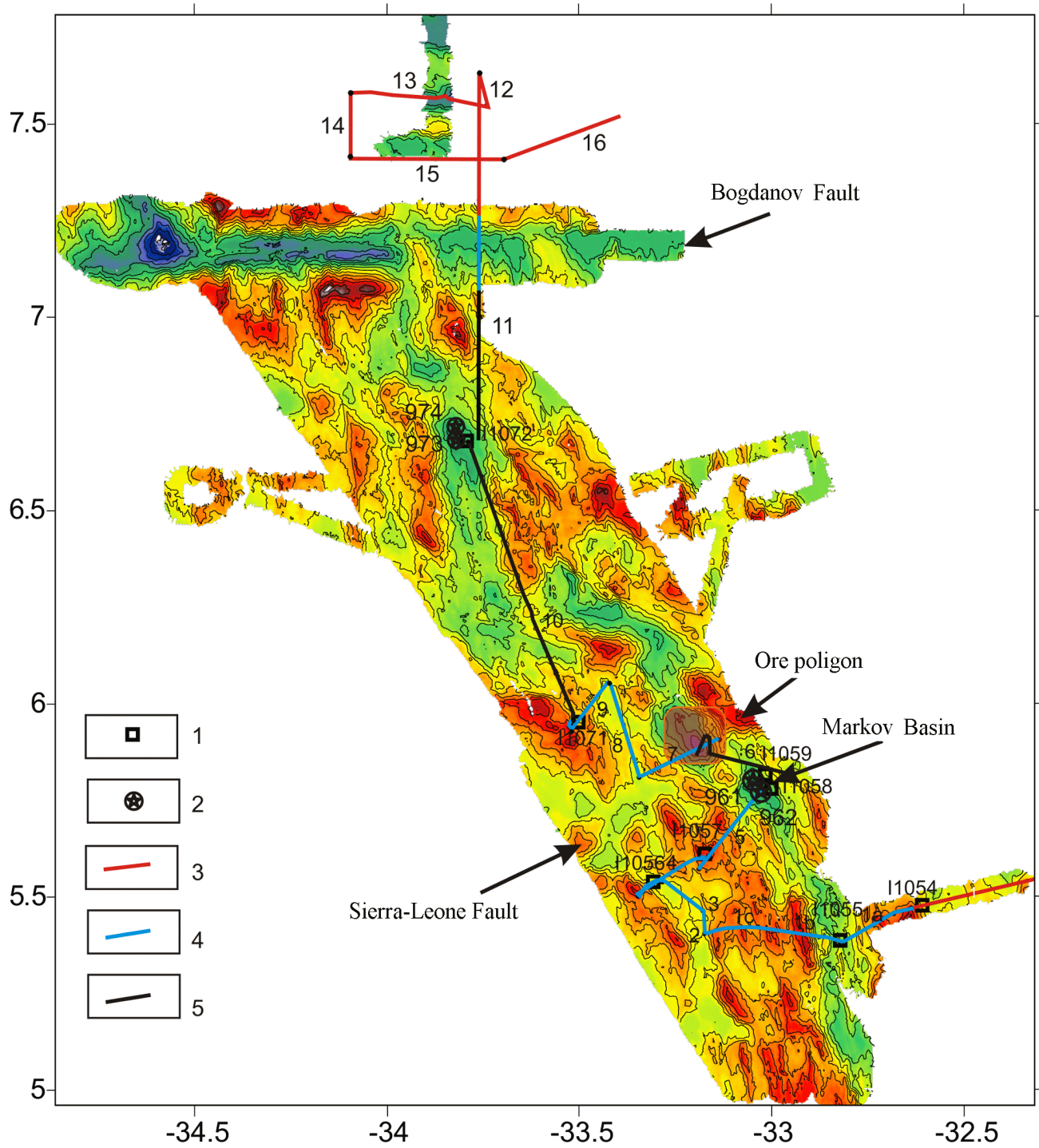


Figure 2. Schematic map of the Sierra Leone MAR segment [after Skolotnev *et al.*, 2003b]. 1 – site of dredging; 2 – site of CTD-sounding; 3–5 – profiles: 3 – multibeam, 4 – parasound, 5 – transition between sites.

layered complex, which is analogous to those in ophiolitic associations like Monviso in the Western Alps [Lombardo *et al.*, 2002].

[9] The abundance of sediments in the axial valley and the

wide occurrence of ultramafics and gabbro indicate that the modern extension of the oceanic crust in this MAR segment proceeded at the predominance of tectonic over magmatic processes. All of the examined and sampled neovolcanic



Figure 3. Primitive leucocratic troctolite, sample I1069/16. Photo: A. A. Peyve.



Figure 5. Plagiogranite (trondhjemite) vein in ilmenite-hornblende dolerite, sample I1060-57. Photo: A. A. Peive.

ridges are variably shifted to the east relative to the rift axis.

General Characterization of the Rocks

[10] The rock samples discussed in this paper were dredged mostly from the slopes of the Markov depression (sites I1032, I1060, I1063, and I1069), and basalts were uplifted from a volcanic plateaus north of it (sites I1026, I1027, and I1072). The dredged material included both fresh and variably altered rock material. The completely metamorphosed rocks were classified into (a) those developing after ultramafic rocks, gabbro, and dolerites and (b) metamorphic rocks.

Petrography

[11] According to their petrographic characteristics, the plutonic rocks can be subdivided into two groups: (i) primitive magnesian troctolites (Figure 3) and gabbro and (ii) gabbronorites and gabbronorite-diorites containing, *Opx*, Fe-Ti oxides, and kaersutite (Figure 4) and associated with norites, pyroxenites, granodiorites and plagiogranites (Figures 5 and Figure 6). As was mentioned above, the latter rocks occur mostly as veins and dikes up to 10–20 cm thick, most often 1–5 cm, and usually contain kaersutite and ilmenite. These rocks seem to typical occur in slow-spreading ridges as such bodies, because they were also found as analogous bodies in other MAR segments [Silant'ev, 1998] and in the Southwest Indian Ridge [Dick et al., 1991; Holm, 2002; Ozawa et al., 1991]. These peridotites are sometimes notably different from mantle residues in bearing relics of

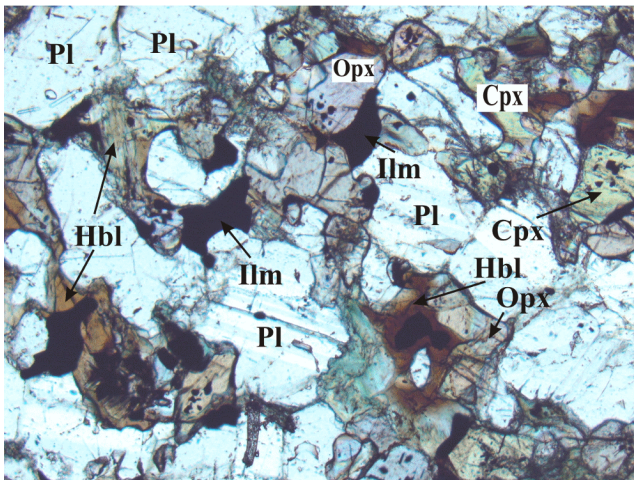


Figure 4. Texture of olivine hornblende gabbronorite with Fe-Ti oxides. Micrograph, thin section I1040-14, magnification 40^x, one polarizer.

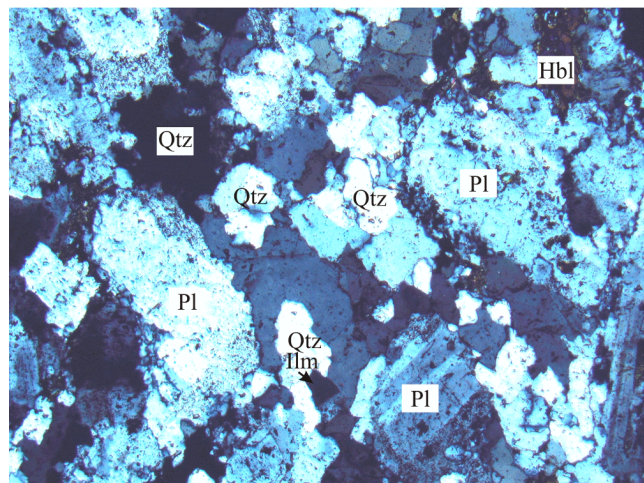


Figure 6. Texture of plagiogranite (trondhjemite). Thin section I1060-57, crossed polarizers.

cumulus textures (Figure 7) and in having different compositions of minerals, particularly chromite (see below), which suggests that the rocks are intrusive.

[12] The dredged dolerite samples are fairly diverse: they include common olivine-clinopyroxene and olivine-free varieties, sometimes with elevated contents of ilmenite (up to 3 vol %), and plagioclase-phyric *Ilm-Hbl* dolerites. Along with fresh rocks, the dredged material contained altered varieties, whose pyroxenes and hornblende are partly or completely replaced by fibrous actinolite.

[13] Both the fresh and the altered basalts can be aphyric or porphyritic, with phenocrysts of *Ol*, *Ol+Pl*, or *Pl* alone. The groundmass of these basalts is usually ophitic or has an unusual texture with sheaves of recrystallized spherulites, which are clearly seen in glassy varieties. The latter type of the basalts usually bears abundant small ilmenite grains, a feature suggesting that these rocks are volcanic analogues of the second group of the plutonic rocks. The rocks often exhibit traces of high-temperature cataclasis with the development of deformation structures in magmatic minerals (*Ol*¹, *Opx*, *Pl*, and *Hbl*) and the appearance of small subequant neoblasts. The genesis of such high-temperature cataclasites was likely related to deformations in already solid but still hot rocks, because the minerals show no traces of low-temperature alterations, and the composition of the neoblasts is close to that of the cataclasts.

[14] Rocks of particular interest are the volcanic breccias that were cataclased under such conditions and were found among rocks from sites I1060 and I1063. Boudin-, oval-, and lens-shaped fragments (15–20 cm long) in these rocks consist of cataclased peridotites with relict cumulus textures (harzburgites and lherzolites) that were not affected by low-temperature alterations and are cemented by weakly cataclased fine-grained porphyritic rocks, whose composition varies from gabbronorite-diorite to granodiorite with ilmenite and magmatic kaersutite. It is worth noting that fragments (boudins) of these ultramafics bear practically no traces of low-temperature alterations at contacts with the diorite-granodiorite cement, as is also typical of relations between syngenetic vein derivatives and their host cumulates.

[15] The low-temperature alterations are spread much more broadly: the peridotites are usually extensively serpentinized, and the gabbroids are amphibolized with the development of fibrous actinolite after pyroxenes and pargasite. The rocks are commonly cut by veinlets of carbonate, prehnite and chlorite. In places, the rocks were also affected by low-temperature shearing and brecciation. The thickest of these zones are associated with the development of diverse metamorphic rocks, which often have disseminated-stringer or massive sulfide mineralization [Pushcharovskii *et al.*, 2002].

[16] In order to characterize the typical varieties of the

¹Mineral symbols: *Ol* – olivine, *Opx* – orthopyroxene, *Cpx* – clinopyroxene (*Aug* – augite), *Pig* – inverted pigeonite, *Pig-Aug* – inverted pigeonite-augite, *Pl* – plagioclase, *Hbl* – brown kaersutitic hornblende, *Qtz* – quartz, *Chl* – chromite, *Ilm* – ilmenite, *Ti-Mag* – titanomagnetite, *Zr* – zircon, *Ap* – apatite, *Am* – amphibole, *Act* – fibrous actinolite; end members: *Fo* – forsterite, *Fa* – fayalite, *En* – enstatite, *Fs* – ferrosilite, *Wo* – wollastonite, *An* – anorthite, *Ab* – albite.

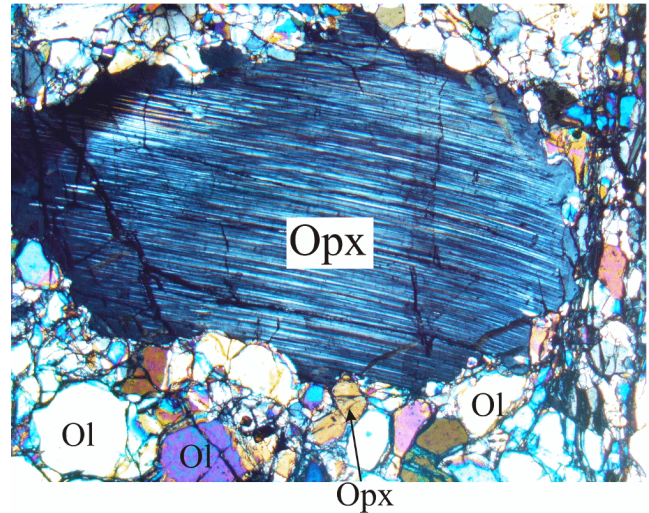


Figure 7. Cumulus orthopyroxene porphyroblast among olivine and pyroxene neoblasts in cataclased lherzolite. Thin section I1063/17, micrograph, magnification 40 \times , crossed polarizers.

rocks, we conducted their detailed petrological and geochemical examination, whose results are summarized below. The petrography of the rocks is briefly characterized in Table 1, and microprobe analyses of their minerals are presented in Tables 2–7.

Chemistry of Major Rock-Forming Minerals

[17] The mineralogy of many of our samples is quite unusual and is generally atypical of both mantle rocks and classic cumulates in continental layered intrusions. First of all, the chemistry of the same minerals varies even within a single thin section, and mineral crystals bear “seed” inclusions that are uncommon in these mineral assemblages.

[18] The composition of olivine in the rocks broadly varies from *Fo*_{91–85} in the peridotites and troctolites to *Fo*₂₆ in the olivine gabbro-diorites (Table 2). A sample of the Fe-Ti-oxide olivine dolerite contains zonal olivine crystals with *Fo*₈₂ in the cores and *Fo*₆₂ in their peripheral portions. The composition of the olivine microphenocrysts in olivine plagioclase-phyric basalt I1072/1 corresponds to *Fo*₈₇, i.e., is close to the composition of olivine in the primitive troctolite. An unusual feature of olivine in the peridotites with relics of cumulate textures is its variable composition: the predominant grains have the composition *Fo*₈₆, and occasional grains correspond to *Fo*₇₀ (sample I1063/17, Table 2).

[19] The composition of pyroxenes from the rocks is demonstrated in Table 3 and Figure 5. A noteworthy feature of the rocks is the presence of unexsolved subcalcic augite (pigeonite-augite). Such pyroxene was found even in the ultramafic rocks (sample I1063/2), a feature absolutely atypical of mantle rocks. It is also pertinent to mention that the composition of the pyroxenes varies even within a single thin section (Figure 8, Table 3).

Table 1. Petrography of the studied samples (minerals contents in vol. %)

no.no./ord.	no. sample	Name of the rock	Texture and mineral composition
1	I1026/21	<i>Pl</i> -phyritic basalt, fresh	<i>Pl</i> phenocrysts, microphenocrysts of <i>Cpx</i> and <i>Ol</i> ; groundmass: mainly <i>Pl</i> with small amount of volcanic glass.
2	I1027/5	Aphiritic plagiobasalt, fresh	Phenocrysts <i>Ol</i> ; groundmass – mainly <i>Pl</i> with small amount of volcanic glass
3	I1032/7	Cataclased <i>Ol</i> gabbro (<i>Ol+Cpx+Pl</i> cumulate)	<i>Ol</i> – 35%, <i>Cpx</i> (<i>Aug</i> – 30%, <i>Pig</i> – 10%), <i>Pl</i> – 30%; small amount of <i>Chr</i> . <i>Ol</i> partly serpentinous, and <i>Pl</i> – partly saussurited.
4	I1060/1	Small-grained dolerite	Microdoleritic texture, formed by <i>Cpx</i> and <i>Pl</i> with small amount (~5–6%) of <i>Ol</i> and 3–4% <i>Ilm</i> . <i>Cpx</i> has specific paniculate texture.
5	I1060/2	Hornblende basalt with <i>Ilm</i>	Fine-porphyritic texture with <i>Pl</i> phenocrysts; groundmass formed mainly by <i>Hbl</i> and <i>Pl</i> with minor <i>Cpx</i> (~10%), <i>Ilm</i> (~1%) and rare <i>Ap</i> .
6	I1060/10	Cataclased coarse-grained gabbro (<i>Pl</i> cumulate)	<i>Pl</i> – 75% (<i>An</i> ₆₅); <i>Cpx</i> : <i>Pig-Aug</i> (<i>W</i> ₂₇ <i>En</i> ₃₉ <i>Fs</i> ₃₄) – 20%, <i>Aug</i> (<i>W</i> ₄₆ <i>En</i> ₄₅ <i>Fs</i> ₉) – 5% (relics within <i>Pig-Aug</i>); <i>Pl</i> often chloritized, pyroxenes partly replaced by fibrous <i>Act</i> .
7	I1060/12	Leucocratic gabbro (<i>Opx+ Cpx+Pl</i> cumulate)	<i>Pl</i> – 70%, <i>Opx</i> – 20%, <i>Cpx</i> – 8%; interstitial <i>Hbl</i> – 2%; <i>Opx</i> partly replaced by talc and fibrous <i>Act</i>
8	I1060/18	Small-grained Fe-Ti-oxide granodiorite	Mineral composition: <i>Pl</i> (<i>An</i> _{10.5}) – 60%, <i>Hbl</i> – 25%, <i>Qtz</i> – 8%, <i>Ilm</i> – 6%, <i>Ap</i> – 1%.
9	I1060/57	Small-grained plagiogranite (trochheimite)	Acid <i>Pl</i> (65%) and <i>Qtz</i> (30%) with small amount (5%) of <i>Hbl</i> and <i>Cpx</i> ; small grains of <i>Ilm</i> , <i>Ap</i> and <i>Zr</i> are presented.
10	I1063/1	Small-grained cataclased Fe–Ti-oxide gabbro	Porphyritic texture with lens-like grains of inverted <i>Pig</i> ; <i>Pl</i> (<i>An</i> ₄₀) – 55%, <i>Cpx</i> (<i>W</i> ₄₁ <i>En</i> ₃₂ <i>Fs</i> ₂₇) – 30%, <i>Opx</i> (<i>W</i> ₃ <i>En</i> ₄₆ <i>Fs</i> ₅₁) – 10%, <i>Ilm</i> – 1%, <i>Mag</i> – 2%, <i>Hbl</i> – 2%; very rare – hyaloserite <i>Fo</i> ₂₆ .
11	I1063/2	Cataclased harzburgite (<i>Ol+Opx+Crt</i> cumulate), non serpentinized	Porphyroclastes of <i>Ol</i> and <i>Opx</i> within fine-grained aggregate neoblasts the same composition: <i>Ol</i> (<i>Fo</i> ₉₁) – 75%, <i>Opx</i> (<i>W</i> ₁ <i>En</i> ₈₇ <i>Fs</i> ₁₂) – 25%, rare <i>Cpx</i> (<i>W</i> ₄₅ <i>En</i> ₄₇ <i>Fs</i> ₈) and <i>Chr</i> .
12	I1063/5	Cataclased Fe–Ti-oxide <i>Hbl</i> gabbro-diorite	Mineral composition: <i>Pl</i> (<i>An</i> ₄₀) – 75%, <i>Hbl</i> – 10%, <i>Cpx</i> (<i>W</i> ₄₃ <i>En</i> ₃₀ <i>Fs</i> ₂₇) – 5%, <i>Opx</i> (<i>W</i> ₂ <i>En</i> ₄₈ <i>Fs</i> ₅₀) – 3%, <i>Ilm</i> – 3%, <i>Ti-Mag</i> – 2%, <i>Ap</i> – 2%. Pyroxenes and <i>Hbl</i> slightly amphibolized with evolving of fibrous <i>Act</i> .
13	I1063/6	Cataclased Fe-Ti-oxide <i>Hbl</i> gabbro	<i>Pl</i> – 60%, <i>Opx</i> – 10%, <i>Cpx</i> – 15%, <i>Hbl</i> – 10%, <i>Ilm</i> – 5%; pyroxenes and <i>Hbl</i> partly replaced by fibrous <i>Act</i> .
14	I1069/16	Leucocratic troctolite (<i>Ol+Pl</i> cumulate)	<i>Ol</i> (<i>Fo</i> ₈₅) – 15%, <i>Pl</i> (<i>An</i> _{76–80}) – 75%, interstitial <i>Cpx</i> (<i>W</i> ₄₅ <i>En</i> ₄₇ <i>Fs</i> ₃₈) – 10%; rare <i>Chr</i> . <i>Ol</i> partly replaced by talc.
15	I1072/1	<i>Ol-Pl</i> basalt with crust of volcanic glass	Small-porphyritic texture. Microphenocrysts <i>Ol</i> (<i>Fo</i> ₈₇) and <i>Pl</i> (<i>An</i> _{71–73}) into the glassy basis; it is found oval xenocrysts of <i>Pl</i> (<i>An</i> _{76–78})
16	L1140/2	<i>Ol-Pl</i> basalt with crust of volcanic glass	Small-porphyritic texture. Needle zonal <i>Pl</i> and microphenocrysts of <i>Ol</i> ; groundmass formed by paniculate grains of <i>Cpx</i> and needles of <i>Pl</i> ; small grains of <i>Ilm</i> present.

Note. *Ol* – olivine, *Opx* – orthopyroxene, *Cpx* – clinopyroxene (augite), *Pig* – pigeonite, *Hbl* – brown magmatic hornblende (pargasite), *Pl* – plagioclase, *Chr* – chromite, *Ilm* – ilmenite, *Mag* – magnetite, *Ap* – apatite, *Act* – actinolite. Composition of minerals studied by microprobe.

Table 2. Representative analyses of olivine in rocks from the Sierra Leone MAR segment

Analyt. spots	SiO ₂	TiO ₂	Al ₂ O ₃	Cr ₂ O ₃	FeO	MnO	MgO	CaO	Na ₂ O	NiO	V ₂ O ₅	P ₂ O ₅	<i>Cl</i>	<i>Fo</i>
I1063/1-6	43.08	0.10	1.06	0.01	45.51	0.50	9.00	0.14	0.43	0.00	0.10	0.01	0.15	0.26
I1063/2-5	42.01	–	–	–	8.60	0.12	48.90	0.04	–	0.33	–	–	–	0.91
I1063/17-2	37.07	0.01	0.05	0.02	26.55	0.43	35.35	0.03	0.14	0.34	0.00	–	0.01	0.70
I1063/17-9	40.66	0.12	0.02	0.04	12.77	0.27	45.95	0.08	0.02	0.07	0.00	0.00	0.00	0.86
I1069/16-4	39.90	0.00	0.13	0.00	14.31	0.11	45.23	0.06	0.11	0.15	0.00	–	0.00	0.85
I1072/1	40.00	–	–	–	12.46	0.21	46.87	0.30	–	0.15	–	–	–	0.87
L1141/15(c)	38.88	0.00	0.00	–	17.41	0.37	42.79	0.38	0.17	–	–	–	–	0.82
L1141/15(r)	36.33	0.16	0.00	–	33.10	0.49	29.53	0.24	0.15	–	–	–	–	0.62

Note. Analyses presented here and below were conducted on a CamScan and Cameca microprobes (at the Moscow State University and the Institute of the Geology of Ore Deposits, Petrography, Mineralogy, and Geochemistry, Russian Academy of Sciences, respectively). All analytical totals are normalized to 100 wt %; dashes mean that the components was not analyzed. Samples: I1063/1 – Fe–Ti-oxide hornblende gabbro; I1063/2 – fresh cataclased harzburgite with relict cumulate textures; I1063/17 – fresh cataclased lherzolite with relict cumulate textures; I1069/16 – fresh leucocratic troctolite (forellenstein); I1072/1 – microphenocrysts from basalt; L1141/15 – Fe–Ti-oxide olivine dolerite, the olivine is zonal: c – core, r – rim of the grain. No zoning was detected in the thin sections.

Table 3. Representative analyses of pyroxenes in rocks from the Sierra Leone MAR segment

Analyt. spots	SiO ₂	TiO ₂	Al ₂ O ₃	FeO	Cr ₂ O ₃	MnO	MgO	CaO	Na ₂ O	K ₂ O	V ₂ O ₅	NiO	P ₂ O ₅	<i>Cl</i>	<i>Wo</i>	<i>En</i>	<i>Fs</i>
I1028/3-1	51.64	0.46	1.77	10.03	–	0.28	13.12	21.84	0.56	0.10	0.07	0.13	–	–	45.4	37.9	16.7
I1028/3-4	51.28	0.92	2.19	12.04	–	0.25	13.23	19.42	0.62	0.00	0.00	0.05	–	–	41.0	38.8	20.2
I1028/3-8	51.70	0.24	0.80	25.57	–	0.47	19.94	0.82	0.33	0.04	0.06	0.00	–	0.02	1.7	57.1	41.2
I1060/3-3	53.30	0.09	0.90	8.68	0.11	0.22	14.41	21.80	0.32	0.06	0.00	0.00	0.03	0.07	44.9	41.2	13.9
I1060/10-1	51.94	0.43	2.58	5.81	0.25	0.26	15.83	22.17	0.36	0.02	0.02	0.20	0.10	0.02	45.5	45.2	9.3
I1060/10-3	52.17	0.15	3.90	18.44	0.01	0.32	12.97	11.16	0.72	0.07	0.00	0.00	0.03	0.07	25.6	41.4	33.0
I1060/10-4	51.54	0.05	3.90	20.42	0.06	0.32	11.26	11.62	0.48	0.06	0.06	0.02	0.17	0.02	28.9	36.2	36.9
I1063/1-1(m)	50.83	0.25	1.25	16.36	0.00	0.58	10.90	19.43	0.34	0.04	0.00	0.00	0.03	0.03	41.0	32.0	27.0
I1063/1-2l	50.07	0.07	0.25	31.68	0.04	0.91	14.22	2.52	0.13	0.02	0.00	0.00	0.08	0.01	5.4	42.0	52.6
I1063/1-7	50.15	0.24	0.50	31.04	0.17	0.71	15.72	1.34	0.00	0.07	0.00	0.00	0.05	0.00	2.8	46.1	51.1
I1063/2-1	56.37	0.03	3.05	5.56	0.50	0.13	33.33	0.97	0.00	0.00	–	0.06	–	–	2.0	89.5	8.5
I1063/2-2	55.71	0.01	2.91	5.75	0.69	0.14	33.86	0.87	0.00	0.00	–	0.06	–	–	1.6	89.8	8.6
I1063/2-4	54.81	0.03	2.48	2.66	0.75	0.06	22.30	16.70	0.18	–	–	0.03	–	–	33.5	62.2	4.3
I1063/2-7	54.21	0.08	1.55	2.16	0.61	0.06	17.72	23.24	0.32	0.00	–	0.05	–	–	46.8	49.7	3.5
I1063/5-2	50.79	0.20	0.90	16.14	0.04	0.55	10.26	20.49	0.30	0.04	0.00	0.18	0.12	0.00	43.3	30.1	26.6
I1063/5-3	54.20	0.06	0.23	27.59	0.01	1.14	15.24	0.99	0.45	0.03	0.00	0.00	0.07	0.00	2.2	48.3	49.3
I1063/5-7	52.73	0.04	0.13	34.65	0.04	0.98	10.00	1.27	0.08	0.05	0.00	0.00	0.00	0.02	3.0	33.0	64.0
I1063/17-2	52.15	0.32	0.87	10.95	0.14	0.26	14.48	20.32	0.33	0.04	0.00	0.00	0.12	0.00	41.5	41.1	17.4
I1063/17-3	52.39	0.12	0.27	23.49	0.06	0.55	21.36	1.47	0.00	0.05	0.04	0.00	0.20	0.00	3.0	60.0	37.0
I1063/17-4	53.78	0.00	1.42	4.17	0.61	0.19	16.32	23.00	0.36	0.00	0.00	0.15	–	0.00	46.8	46.3	6.9
I1063/17-5	51.92	0.29	0.75	13.50	0.01	0.39	12.52	20.06	0.39	0.02	0.00	0.00	0.13	0.01	41.8	36.2	22.0
I1063/17-6	56.38	0.05	1.72	7.50	0.60	0.30	32.82	0.52	0.00	0.00	0.00	0.08	–	0.04	1.0	87.3	11.7
I1063/17-10(m)	51.69	0.01	4.43	2.37	1.41	0.05	16.06	23.17	0.40	0.04	0.00	0.21	0.15	0.02	48.9	47.2	3.9
I1063/17-11(l)	54.64	0.13	4.16	6.27	1.08	0.11	32.34	0.61	0.35	0.07	0.00	0.14	0.08	0.01	1.1	89.2	9.7
I1063/17-12	56.40	0.00	2.56	5.63	0.76	0.25	32.55	1.72	0.00	0.00	0.00	0.02	0.04	0.07	3.3	88.2	8.5
I1069/16-2	51.82	0.45	3.14	4.19	1.13	0.05	16.16	22.58	0.24	0.05	0.00	0.10	0.10	0.00	46.7	46.6	6.7
L1141/15	53.03	0.05	2.55	4.21	0.00	0.13	16.44	23.38	0.21	0.00	–	–	–	–	44.8	49.7	5.5
L1163/34-1	51.34	0.57	1.83	13.95	–	0.40	10.86	20.71	0.31	–	–	0.03	–	–	44.0	32.1	23.8
L1163/34-9	50.53	0.52	1.49	13.71	–	0.44	11.44	21.55	0.29	–	–	0.03	–	–	44.4	32.8	22.8
L1163/34-3	52.32	0.27	0.53	27.51	0.06	0.74	16.40	2.14	–	–	–	0.03	–	–	4.5	48.6	46.9
L1163/34-7	51.16	0.30	0.62	29.83	–	0.78	15.60	1.63	–	–	–	0.05	–	–	3.5	45.9	50.6

Note. All analytical totals are normalized to 100 wt %. Samples: I1028/3 – Fe–Ti-oxide gabbro; I1060/3 – hornblende dolerite; I1060/10 – coarse-grained gabbro, I1063/1 – Fe–Ti-oxide hornblende gabbro; I1063/2 – fresh cataclased harzburgite; I1063/5 – Fe–Ti-oxide hornblende gabbro-diorite; I1063/17 – fresh cataclased lherzolite (m – rock matrix, l – lamella); I1069/16 – fresh troctolite, L1141/15 – Fe–Ti-oxide olivine dolerite; L1163/34 – Fe–Ti-oxide gabbro.

Table 4. Representative analyses of plagioclase in rocks from the Sierra Leone MAR segment

Analyt. spots	SiO ₂	TiO ₂	Al ₂ O ₃	FeO	MnO	MgO	CaO	Na ₂ O	K ₂ O	Cl	Cr ₂ O ₃	V ₂ O ₅	NiO	P ₂ O ₅	Or	Ab	An
I1028/3-5	56.47	0.00	27.38	0.18	0.00	0.10	9.55	6.20	0.11	–	–	–	–	–	0.6	53.7	45.7
I1028/3-2	56.14	0.14	27.31	0.30	0.01	0.03	9.48	6.24	0.22	–	–	–	0.13	–	1.3	53.7	45.0
I1060/3-1	47.65	0.00	32.59	0.33	0.00	0.08	16.62	2.42	0.04	0.02	0.00	0.01	0.12	0.12	0.2	20.9	78.9
I1060/3-2	51.59	0.00	30.28	0.16	0.00	0.00	13.62	3.97	0.96	0.02	0.19	0.00	0.01	0.07	0.5	34.4	65.1
I1060/18-3	67.27	0.00	20.75	0.00	0.05	0.00	1.98	9.72	0.03	0.00	0.10	0.03	0.02	0.06	0.05	89.5	10.5
I1060/63-1	60.70	0.09	24.70	0.23	0.00	0.06	6.13	7.71	0.23	0.04	–	0.00	0.12	–	1.3	68.5	30.1
I1063/1-8	58.71	0.01	25.42	0.30	0.00	0.07	8.19	6.60	0.14	0.00	0.00	0.00	0.12	0.43	0.8	58.9	40.3
I1063/1-10	57.74	0.07	26.10	0.08	0.00	0.00	8.66	6.69	0.20	0.03	0.16	0.00	0.15	0.12	1.1	57.7	41.2
I1063/5-1	58.32	0.05	25.78	0.25	0.11	0.00	8.22	6.91	0.085	0.03	0.10	0.00	0.00	0.13	0.5	60.0	39.5
I1063/17-1	60.39	0.02	25.16	0.01	0.00	0.00	6.88	7.33	0.21	0.01	0.00	0.00	0.00	–	1.3	65.0	33.7
I1063/17-4	60.16	0.00	24.67	0.11	0.00	0.00	7.04	7.48	0.15	0.01	0.05	0.00	0.07	0.26	0.1	65.0	33.9
I1063/17-14	54.03	0.00	28.57	0.21	0.00	0.08	11.58	5.17	0.00	0.00	0.28	0.00	0.00	0.08	–	44.7	55.3
I1069/16-2(l)	49.68	0.04	31.57	0.18	0.00	0.05	15.58	2.69	0.02	0.03	0.00	0.00	0.00	0.07	0.1	23.8	76.1
I1069/16-3(s)	47.73	0.08	32.73	0.29	0.00	0.03	16.45	2.21	0.08	0.05	0.05	0.07	0.00	0.03	0.5	19.3	80.2
I1072/1(x)	49.08	–	32.26	0.25	–	–	15.90	2.51	–	–	–	–	–	–	–	22.2	77.8
I1072/1(l)	50.65	–	31.20	0.42	–	–	14.68	3.05	–	–	–	–	–	–	–	27.3	72.7
I1072/1(l)	50.54	–	31.31	0.38	–	–	14.50	3.27	–	–	–	–	–	–	–	29	71
L1141/15(c)	51.30	0.00	30.37	0.56	0.00	0.00	14.20	3.49	0.08	–	–	–	–	–	0.4	31.0	68.6
L1141/15 (r)	55.66	0.14	27.42	0.79	0.00	0.00	10.50	5.36	0.13	–	–	–	–	–	0.7	47.5	51.6
L1163/34-14	57.12	–	26.95	–	0.25	–	9.30	6.32	0.06	–	–	–	–	–	0.3	55.0	44.7
L1163/34-18	57.50	–	26.84	–	0.24	–	8.94	6.41	0.07	–	–	–	–	–	0.4	56.2	43.4

Note. All analytical totals are normalized to 100 wt %. Samples: I1028/3 – Fe–Ti-oxide hornblende gabbro; I1060/3 – plagioclase-phyric hornblende dolerite (I1060/3-1 – aggregate of phenocrysts, I1060/3-2 – thin lath); I1060/18 – granodiorite; I1060/63 – hornblende quartz diorite; I1063/1 – hornblende gabbro (I1063/1-8 – subhedral crystal, I1063/1-10 – inclusion in clinopyroxene); I1063/5-1 – Fe–Ti-oxide hornblende gabbro-diorite; I1063/17-1 and I1063/17-4 – thin granodiorite vein; I1063/17-14 – hercynite (rim around chromite); I1069/16 – troctolite, cumulate plagioclase; I1069/16-2(s) – large individual grain, I1069/16-3(l) small chadacryst in clinopyroxene oikocryst; I1072/1 – basalt: x – xenocryst, l – lath; L1141/15 – dolerite (c – core, r – rim); L1163/34 – Fe–Ti-oxide gabbro.

Table 5. Representative analyses of kaersutite in rocks from the Sierra Leone MAR segment

Analyt. spots	SiO ₂	TiO ₂	Al ₂ O ₃	FeO	MnO	MgO	CaO	Na ₂ O	K ₂ O	V ₂ O ₅	NiO	Cl	Cr ₂ O ₃	P ₂ O ₅
I1028/3-5	46.56	1.63	8.85	13.74	0.14	13.99	12.01	2.36	0.08	0.42	0.23	–	–	–
I1028/3-6	46.47	1.63	8.83	13.72	0.14	13.96	12.00	2.36	0.08	0.42	0.23	0.17	–	–
I1028/3-9	46.44	1.77	8.94	12.85	0.03	14.33	12.40	2.18	0.15	0.45	0.21	0.26	–	–
I1060/3-5	48.25	1.76	8.23	12.88	0.21	14.80	11.35	1.98	0.22	0.11	0.10	0.00	0.00	0.10
I1060/18	46.55	1.35	5.36	29.68	0.50	4.82	9.69	1.46	0.36	0.08	0.00	0.10	0.01	–
I1063/1-11	44.95	2.08	9.38	18.78	0.25	10.65	11.00	2.50	0.17	0.09	0.04	0.00	0.01	0.10
I1063/2	51.92	1.06	4.41	14.75	0.20	15.36	11.16	0.81	0.12	0.16	0.17	0.06	0.09	–
I1063/17-5	46.65	0.32	11.89	5.95	0.09	18.20	12.08	2.86	0.21	0.00	0.04	0.00	1.71	0.03
I1063/17-6	45.08	3.53	10.35	12.26	0.02	14.08	11.12	2.78	0.24	0.03	0.21	0.02	0.13	0.14
I1068/33-3	49.50	1.23	9.09	7.44	0.02	18.26	11.59	2.20	0.30	0.05	0.00	0.05	0.27	–
L1124/13-1	49.16	2.39	8.39	18.03	0.30	11.52	10.16	2.49	0.24	–	–	0.05	–	–
L1163/34-11	49.98	0.58	6.78	20.37	0.34	9.64	11.09	1.08	0.11	–	0.03	–	–	–
L1163/34-12	48.20	1.20	8.71	19.96	0.26	8.96	10.91	1.59	0.18	–	0.03	–	–	–
L1163/34-13	51.77	0.65	5.31	19.36	0.32	10.39	11.17	0.92	0.08	–	0.03	–	–	–

Note. All analytical totals are normalized to 100 wt %. Samples: I1028/3 – hornblende gabbro; I1060/3 – plagioclase-phyric hornblende dolerite; I1060/18 – ilmenite–hornblende granodiorite; I1063/1 – Fe–Ti-oxide hornblende gabbro; I1063/17 – thin vein of two-pyroxene hornblende granodiorite; I1068/33 – coarse-grained gabbro; L1124/13 – hornblende gabbro; L1163/34 – hornblende gabbro.

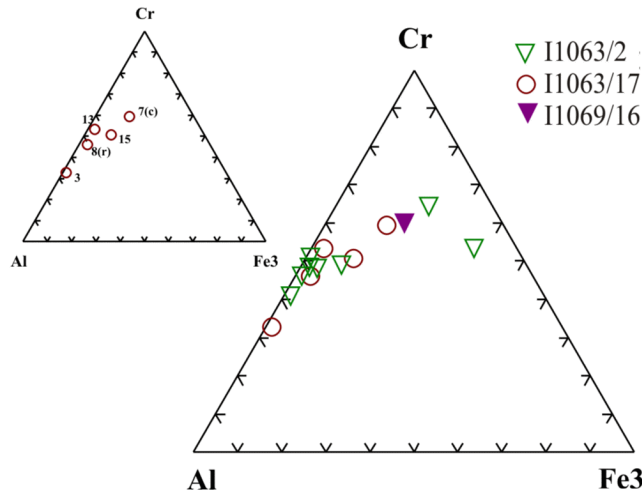


Figure 8. Cr–Al–Fe³⁺ diagram for the composition of chromite from the rocks.

[20] The composition of the plagioclase varies within broad ranges, from bytownite An_{80} to oligoclase-albite An_{10} . Basalt I1072/1 contains plagioclase xenocrysts of composition An_{76-78} and microcrysts of composition An_{71-73} . A notable feature of plagioclase in these rocks is its very low K contents (Table 4, Figure 9).

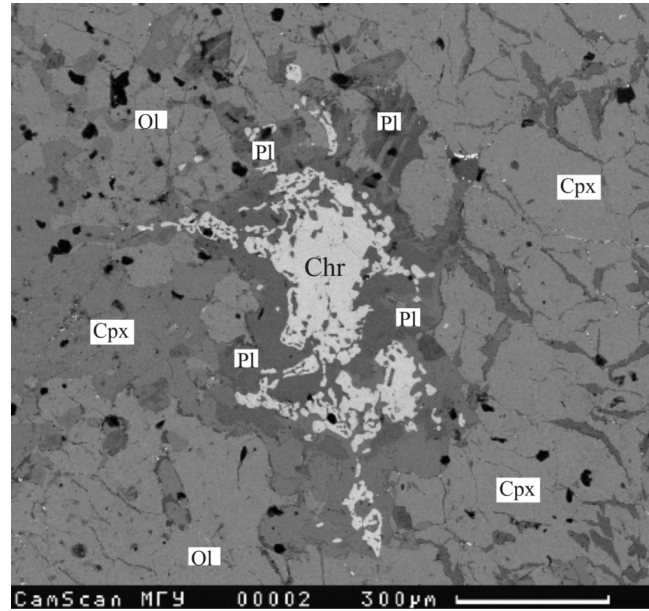


Figure 10. Corroded Cr-spinel grain (Table 6, analysis I1063/17-15) in ilherzolite I1063/17. The grain is surrounded by small grains of plagioclase ($An_{55.3}$; Table 4, analysis I1063/17-14). Darker gray corresponds to clinopyroxene, paler gray is olivine, and black patches are remnants of the carbon sputter coating. BSE image, CamScan electron microscope, Moscow State University.

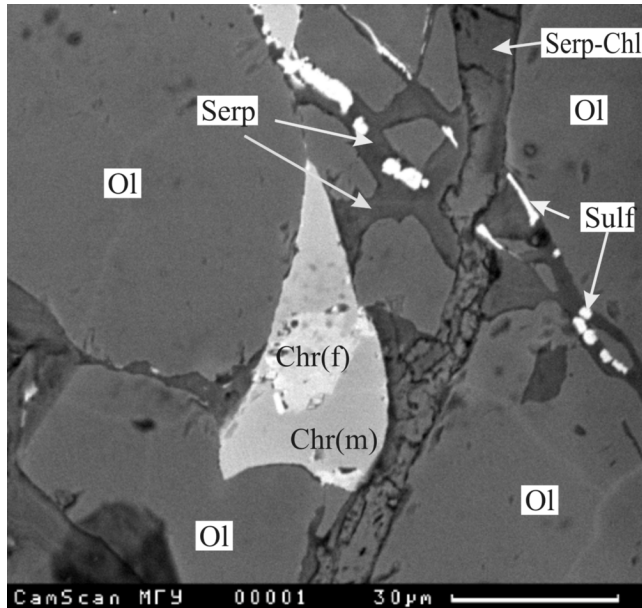


Figure 9. Zonal chromite grain in ilherzolite I1063/17. The brighter central part of the grain corresponds to Fe-rich chromite (Table 6, analysis I1063/17-7(c)), and its grayish peripheral part corresponds to Mg-rich chromite (Table 6, analysis I1063/17-8(r)); dark gray grains are olivine. The sample is cut by serpentine veinlets with small magnetite grains (white) and a younger serpentine–chlorite veinlet. BSE image, CamScan electron microscope, Moscow State University.

[21] Magmatic kaersutitic brown hornblende occurs in the gabbroids both as a cumulus mineral and as intercumulus grains, and the dolerites contain small kaersutite grains in the groundmass. Similarly to the pyroxenes, the hornblende is often replaced by fibrous actinolite. The composition of the hornblende varies from high-Ti varieties in the hornblende gabbroids to relatively low-Ti varieties in the diorites and quartz diorites (Table 5). According to the results of *Pl-Am* thermometry [Blundy and Holland, 1990], the rock crystallized at temperatures from 800°C (Fe-Ti-oxide hornblende gabbro-diorite L1124/13-11) to 650–580°C (Fe-Ti-oxide gabbro-diorite and quartz diorite) (unpublished data of S. S. Abramov).

[22] The apatite contains small amounts of Cl (0.09–0.24 wt%). Fluorine was not determined in this mineral because of methodical difficulties.

[23] The oxide minerals (Cr-spinel, titanomagnetite, and ilmenite) are particularly interesting as exhibiting some noteworthy structural features.

[24] A remarkable feature of Cr-spinel in our samples of the cataclased peridotites with relics of cumulate textures is its broad chemical variations (Table 6, Figure 10), which are atypical of this mineral in mantle rocks but is typical of Cr-spinel in the cumulates of layered intrusions. Moreover, some chromite grains have corroded cores (Figure 11) consisting of Fe-rich chromite and surrounded by more magnesian peripheral zones, which contain P and Cl (Table 6).

[25] It is also worth mentioning the development of rims of fine-grained plagioclase $An_{55.3}$ around a resorbed chromite

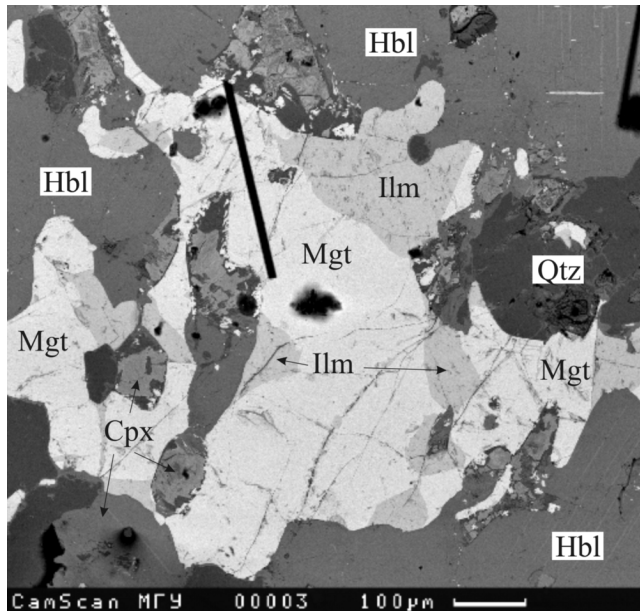


Figure 11. Character of ilmenite and magnetite crystallization in Fe-Ti-oxide hornblende gabbro-diorite I1063/1. Brightest white—magnetite (Table 7, analysis I1063/1-3), darker grayish white—ilmenite (Table 7, analysis I1063/1-4), gray—brown hornblende (partly chloritized), dark gray—augite with thin orthopyroxene lamellae, almost black—quartz. BSE image, CamScan electron microscope, Moscow State University.

grain (Figure 12), whose composition is close to that of the zonal chromite grain described above in the same thin section (Table 4, analysis I1063/17-14). The outer part of this rim consists of fine clinopyroxene grains, and the grain itself is located among olivine neoblasts. Similar rims often develop around chromite grains during high-temperature

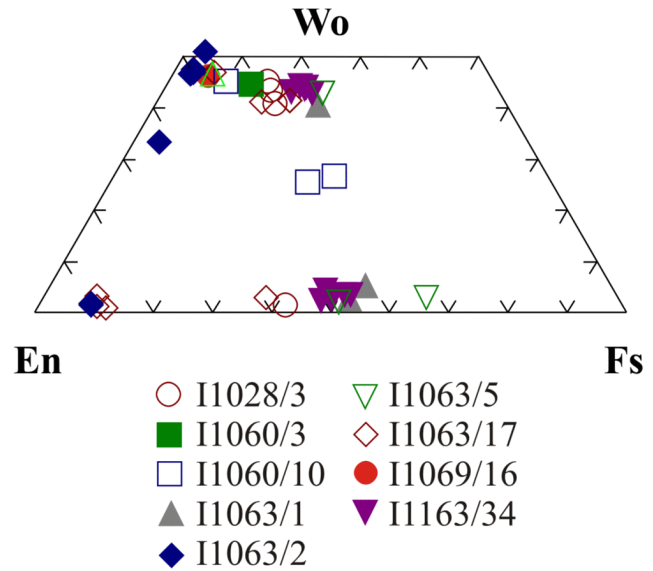


Figure 12. Fragment of a triangular Wo-En-Fs plot showing the composition of pyroxenes from the studied rocks.

and low-pressure transformations in ultramafics occurring in ophiolitic associations [Laz'ko and Sharkov, 1988].

[26] The composition of most chromite grains in this thin section and the chemistry of the vermicular aggregates among olivine and pyroxene neoblasts, as well as the composition of chromite in the rim of the zonal crystal, are characterized by very low Fe^{3+} contents and variable Cr/Al ratios. As in this rock, Cr-spinels in harzburgite I1063/2 can be subdivided into two groups: one close to the predominant type of grains in sample I1063/17, and the other characterized by low Al_2O_3 contents and high concentrations of Cr_2O_3 .

Table 6. Representative analyses of Cr-spinel in rocks from the Sierra Leone MAR segment

Analyt. spots	SiO ₂	TiO ₂	Al ₂ O ₃	Cr ₂ O ₃	FeO	MnO	MgO	CaO	Na ₂ O	K ₂ O	V ₂ O ₅	NiO	ZnO	P ₂ O ₅	Cl
I1030/1-1	—	0.85	24.33	40.00	19.49	0.13	15.20	—	—	—	—	—	—	—	—
I1030/1-2	—	0.88	24.55	40.08	19.44	0.13	14.92	—	—	—	—	—	—	—	—
I1063/2-1	—	0.17	26.45	41.88	19.45	n.d.	11.29	—	—	—	0.38	0.09	0.29	—	—
I1063/2-2	—	0.08	29.73	38.81	18.09	n.d.	12.67	—	—	—	0.31	0.09	0.22	—	—
I1063/2-3	—	0.03	33.23	35.40	16.94	n.d.	13.68	—	—	—	0.38	0.13	0.21	—	—
I1063/2-4	—	0.33	6.96	46.06	40.85	0.82	3.08	—	—	—	0.48	0.11	1.32	—	—
I1063/2-5	—	0.94	4.61	37.12	52.32	0.64	2.70	—	—	—	0.55	0.20	0.92	—	—
I1063/17-3	0.29	0.05	38.64	28.97	16.35	0.06	15.00	0.00	0.42	0.00	0.06	0.16	—	—	—
I1063/17-7(c)	0.35	0.11	12.89	43.33	38.72	0.31	3.36	0.09	0.77	0.13	0.37	0.00	—	0.00	0.00
I1063/17-8(r)	0.00	0.00	27.32	37.38	24.13	0.35	9.43	0.07	0.62	0.00	0.37	0.00	—	0.18	0.04
I1063/17-13	0.14	0.06	23.60	42.89	22.09	0.46	10.06	0.07	0.35	0.01	0.24	0.00	—	0.00	0.02
I1063/17-15	0.03	1.17	19.08	37.56	36.31	0.19	4.67	0.08	0.61	0.02	0.22	0.00	—	0.00	0.07
I1069/16-1	0.00	1.83	10.13	41.37	42.66	0.53	2.48	0.04	0.29	0.00	0.61	0.00	—	0.00	0.06

Note. All analytical totals are normalized to 100 wt %. Samples: I1030/1 – basaltic glass; I1063/2 – cataclased harzburgite with relict features of a cumulate texture; I1063/17 – cataclased lherzolite with relict features of a cumulate texture (c – inner part of the grain, r – its peripheral portion (see Figure 4); I1063/17-13 – vermicular grain; I1063/17-15 – chromite with a reaction rim of columnar plagioclase grains); I1069/16 – fresh leucocratic troctolite (forellenstein); n.d. – not determined.

Table 7. Representative analyses of Fe–Ti oxides and apatite in rocks from the Sierra Leone MAR segment

Analyt. spots	SiO ₂	TiO ₂	Al ₂ O ₃	Cr ₂ O ₃	Fe ₂ O ₃	FeO	MnO	MgO	CaO	Na ₂ O	K ₂ O	V ₂ O ₅	NiO	Cl	P ₂ O ₅
I1028/3-3	0.06	49.85	0.08	0.00	–	48.40	0.71	0.58	0.03	0.00	0.02	0.00	0.26	0.00	0.00
I1060/3-1	0.15	51.28	0.05	0.12	–	45.57	2.36	0.15	0.10	0.00	0.00	0.14	0.00	0.04	0.04
I1060/18-2	0.04	51.40	0.11	0.10	–	46.78	1.30	0.12	0.06	0.00	0.00	0.04	0.00	0.03	0.02
I1060/18-4(ap)	0.37	0.12	0.02	0.01	–	0.30	0.06	0.00	56.36	0.44	0.05	0.00	0.03	0.26	41.98
I1060/63-3	0.21	50.04	0.22	0.03	–	46.84	0.50	1.51	0.35	0.02	0.06	0.19	0.00	0.04	0.00
I1063/1-3	0.16	9.76	2.75	0.15	39.53	45.55	0.19	0.33	0.11	0.52	0.00	0.90	0.00	0.05	0.00
I1063/1-4	0.07	51.62	0.03	0.07	–	47.16	0.93	0.00	0.05	0.00	0.02	0.00	0.00	0.05	0.00
I1063/1-9(inc)	0.09	12.37	1.50	0.11	41.68	42.64	0.37	0.34	0.09	0.43	0.01	0.33	0.00	0.04	0.00
I1063/5-4	0.08	50.44	0.10	0.03	–	47.40	1.40	0.14	0.00	0.27	0.00	0.00	0.00	0.00	0.14
I1063/5-5	0.02	3.29	0.92	0.00	33.98	61.51	0.00	0.17	0.01	0.06	0.00	0.00	0.00	0.01	0.03
I1063/17-1	0.11	51.66	0.17	0.16	–	45.67	0.65	0.97	0.07	0.15	0.00	0.00	0.01	0.01	0.38
I1063/17-7	0.27	52.08	0.09	0.34	–	45.80	0.95	0.00	0.26	0.00	0.03	0.00	0.15	0.03	0.00
I1063/17-8(ap)	0.44	0.00	0.00	0.00	–	0.14	0.05	0.00	56.29	0.00	0.12	0.00	0.00	0.09	42.87
L1163/34-26	–	8.85	3.35	0.07	38.46	48.04	0.95	0.28	–	–	–	–	–	–	–
L1163/34-29	–	52.92	0.04	–	–	45.83	0.96	0.25	–	–	–	–	–	–	–

Note. All analytical totals are normalized to 100 wt %. Samples: I1028/3 – hornblende gabbro-norite with ilmenite; I1060/3 – hornblende dolerite; I1060/18 – granodiorite; I1060/63 – fine-grained hornblende dolerite with ilmenite; I1063/1 – Fe–Ti-oxide hornblende gabbro-norite (3 – zonal grain, analyzed by scanning over an area, 4 – Ilm grain, 9 – inclusion in clinopyroxene with exsolution lamellae); I1063/5 – Fe–Ti-oxide hornblende gabbro-diorite; I1063/17 – gabbro-norite-diorite veinlet in lherzolite; L1163/34 – Fe–Ti-oxide gabbro-norite; ap – apatite; inc – inclusion.

[27] All of these data evidently indicate that the early Fe-rich chromite with elevated TiO₂ and relatively low Al₂O₃ and MgO contents are xenogenic for these peridotites. They could be preserved as inclusions in other minerals (when captured by growing crystals), but more commonly they reacted with the magmatic melt and were dissolved in it. Likely evidence of this processes is displayed in Figure 12.

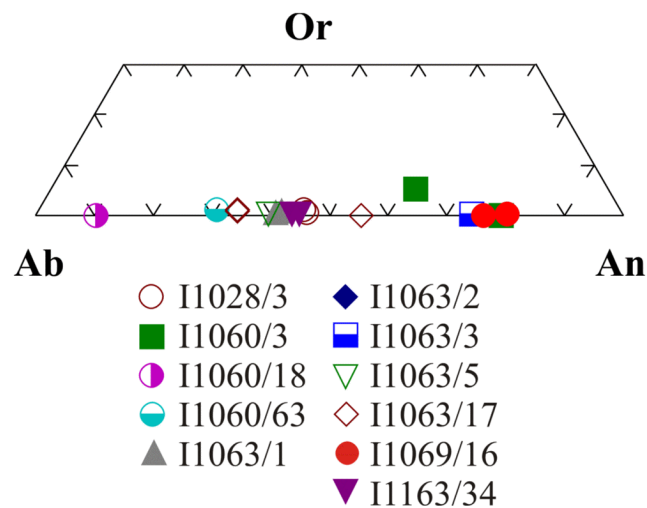
[28] The Fe–Ti oxides of the rocks are unusual. For example, titanomagnetite with exsolution ilmenite lamellae, which are typical of continental mafic intrusions [Bogatikov, 1996; Wager and Brown, 1968], is contained in the gabbro-norites only in the form of small inclusions in clinopy-

roxene. These oxides (*Mag* containing <10 wt % TiO₂ and *Ilm*) usually crystallize together or compose individual grains (Table 7, Figure 13). According to Fershtater *et al.* [2001], this mode of occurrence of Fe–Ti oxides is typical of rocks that crystallized from hydrous melts at relatively low temperatures (600–800°C, $-\log f_{O_2} = 8-11$).

[29] As obviously follows from all of these data, the rocks contain minerals belonging to at least two distinct assemblages. Relics of the earlier of them are contained as inclusions (“seeds”) in the typical minerals of the magmatic assemblage itself. These are Fe-rich *Chl* overgrown by rims of a more magnesian and less titanian variety in the peridotite (sample I1063/17) and Ti-*Mag* with exsolution lamellae in clinopyroxene from the gabbro-norite (sample I1063/1). Moreover, the composition of the olivine significantly varies, and volumetrically predominant magnesian varieties are in places associated with moderately magnesian grains. All of these facts testify to very unusual conditions under which the rocks were produced.

[30] A noteworthy feature of the rocks is the variable composition of the same minerals in them. This can be illustrated most glaringly by the example of the peridotites with relict cumulus textures: a single sample of these rocks can contain olivine of the composition For_{86} and For_{70} (Table 2, sample I1063/17). The broadest compositional variations in this sample and in I1063/2 are exhibited by their Cr-spinel (Table 6, Figure 10). Some of their grains are Fe-rich, which is atypical of mantle rocks but is characteristic of ultramafic layered complexes [Sharkov *et al.*, 2001]. Moreover, some of the chromite grains contain corroded cores of Fe-rich chromite overgrown by more magnesian outer zones, which contain P and Cl (Figure 11, Table 6).

[31] As can be seen from Table 8, the Fe–Ti-oxide gabbro-norites crystallized, according to *Ilm-Mag* geothermometry,

**Figure 13.** Composition of plagioclase in the rocks.

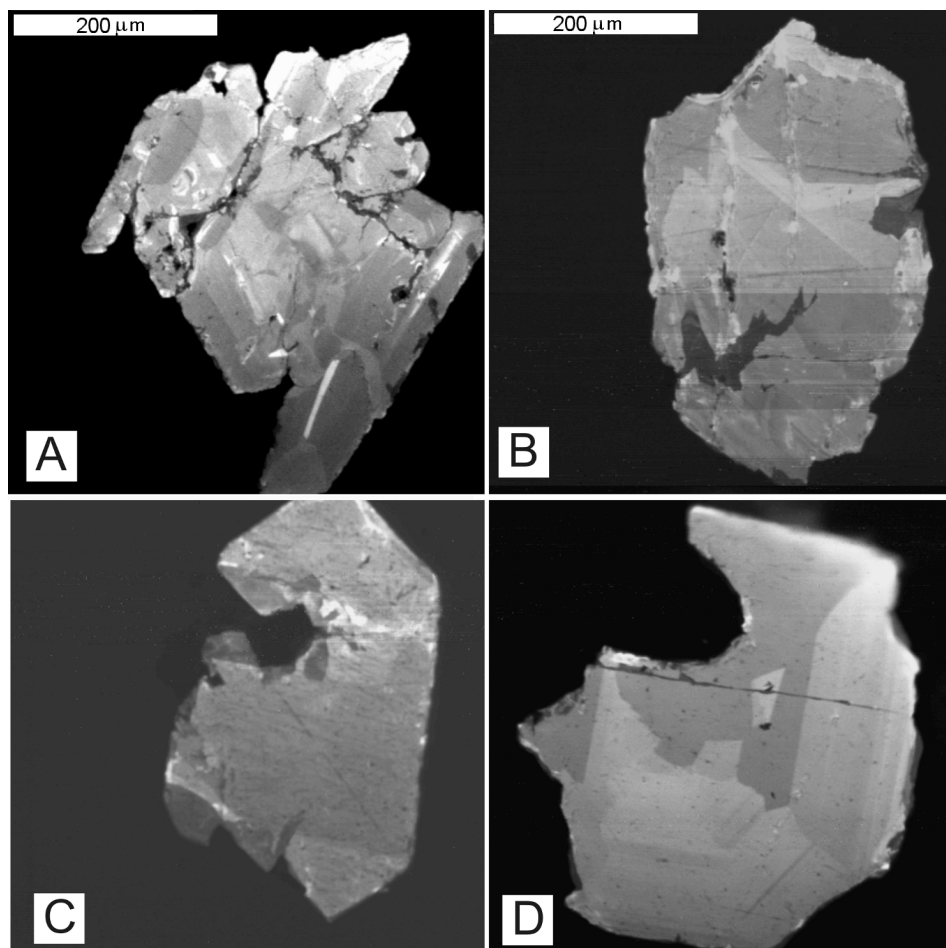


Figure 14. Morphology and inner structure of zircon grains from sample I1028/1 (cathode luminescence data). Determinations were conducted at the University of Granada, Spain. A, B – Fragments of deformed zircon grains with sectorial zoning; C – dipyramidal zircon grain with cross zoning; D – fragment of a zircon grain whose inner part has a sectorial zoning and the outer rim exhibits oscillatory zoning.

at average temperatures of $621 \pm 41^\circ\text{C}$, which is close to the analogous values obtained by the same method for Fe-Ti-oxide gabbroids in the Southwest Indian Ridge [Natland *et al.*, 1991].

U-Pb Age of the Rocks

[32] As was mentioned above, the Fe-Ti-oxide rocks contain zircon. Zircon for radiological dating was separated from one of our rock samples (cataclased hornblende gabbro-norite, sample I1028/1, dredged from the rift valley wall at a depth of close to 4 km). The rock was dominated by clinopyroxene and plagioclase and contained subordinate amounts of orthopyroxene, magmatic brown hastingsitic hornblende, ilmenite, and accessory apatite and zircon. Cataclasis resulted in this rock in the deformations of large crystals (cloudy extinction and deformed twinning boundaries in plagioclase and bent exsolution lamellae in pyroxenes) and the development of small subequant neoblasts. The zircon was also cataclased and disintegrated into small fragments. The

secondary alterations were generally insignificant and involved the replacement of mafic minerals by fibrous actinolite.

[33] Analogous rocks were dredged from the walls of other parts of the Markov depression and neighboring depressions in this MAR segment, which testifies to their broad *in-situ* occurrence. Zircon grains were obtained from sample I1028/1 using magnetic separation and heavy liquids, and by hand-picking under a binocular magnifier. The grains were classified according to their size, color, and morphology. Approximately 70–75% of each population were utilized to prepare epoxy pellets, which were polished and examined under an electron microscope with a cathode-luminescence detector. The rest of the populations were dated (TIMS) by the U-Pb method [Sharkov *et al.*, 2004a].

[34] The largest fraction ($\geq 450 \times 250 \mu\text{m}$) consisted of colorless transparent and semitransparent zircon grains disintegrated into small fragments during cataclasis (Figure 14). The weak erosion of their face surfaces suggests that the zircon was partly dissolved. The cathode luminescence examination of more than 30 individual zircon grains revealed their

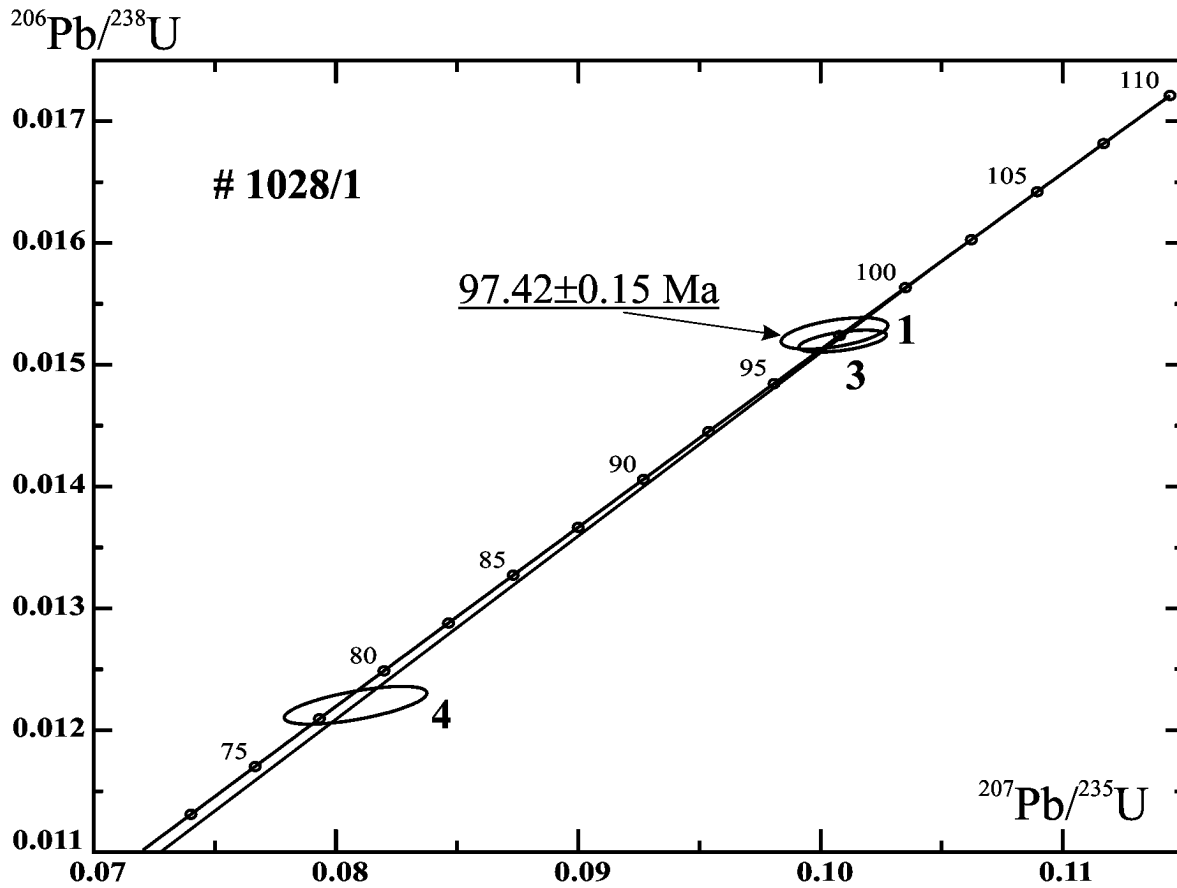


Figure 15. Isochron diagram.

zoning, which is likely of magmatic genesis. We detected weak oscillatory and peculiar sectorial zoning (Figures 14a, 14b), as is typical of zircon from mafic crystalline rocks, particularly those in ophiolitic complexes [Rubatto and Gebauer, 2000]. The primary nature of the sectorial zoning is clearly seen in Figure 2c, in which a fragment of this zoning cuts across the morphological features of a small fragment crystal of a zircon crystal.

[35] The smaller fraction includes euhedral zircon grains with clearly pronounced dipyrmaid faces (Figure 14c). The predominance of euhedral grains was caused both by the crystallization of this zircon from a melt and by the fragmentation of larger grains during cataclasis. This follows from the fact that the zoning of some grains is not conformable with their morphology (Figure 2c), whose euhedral faceting

seems to be secondary and imitates the habit of the larger primary grain.

[36] Zircon dating was conducted on a Finnigan MAT-261 solid-source eight-collector mass spectrometer using samples of three size fractions of the most transparent and euhedral grains and grain fragments. Fraction I consisted of 18 grains, which ranged from 500 μm to 300 μm along the long axis and from 250 μm to 150 μm along the short one. Fraction III comprised 35 grains with average sizes of 250 \times 175 μm , and fraction IV included 30 grains and grain fragments with average sizes of 250 \times 140 μm . A subcordant age value was obtained for small and the most euhedral and transparent crystals (Figure 15, Table 9). The age of the rock is 97.42 \pm 0.15 Ma.

[37] Our experience in studying zircon from blastomyloni-

Table 8. Ilmenite-magnetite thermometry of Fe–Ti-oxide gabbronorites and gabbronorite-diorites

Analyses in Table 5	[Powell and Powell, 1977]	[Spenser and Lindsley, 1981]	[Andersen and Lindsley, 1985]
I1063/1-3 and I1063/1-4	588–605°C;	510–545°C; – lg $f\text{O}_2$ = 24.34 – 26.40	539–572°C; – lg $f\text{O}_2$ = 25.32 – 25.40
I1063/5-4 and I1063/5-5	542–543°C;	586–590°C; – lg $f\text{O}_2$ = 20.76 – 20.90	607–608°C; – lg $f\text{O}_2$ = 20.28 – 20.39
L1163/34-27 and L1163/34-29		571–580°C	601–613°C

Table 9. U-Pb isotopic dating of zircon from cataclased hornblende gannronorite, sample II028/1, Markov depression, Central Atlantic

no.	sample (mg)	[Pb] _{rad} ppm	[U] ppm	²⁰⁶ Pb/ ²⁰⁴ Pb	²⁰⁷ Pb/ ²⁰⁶ Pb	²⁰⁸ Pb/ ²⁰⁶ Pb	²⁰⁶ Pb/ ²⁰⁶ Pb	²⁰⁷ Pb/ ²³⁵ U (2σ%)	²⁰⁶ Pb/ ²³⁸ U (2σ%)	Rho	Age ²⁰⁷ Pb/ ²³⁵ U (Ma)	Age ²⁰⁶ Pb/ ²³⁸ U (Ma)	Age ²⁰⁷ Pb/ ²⁰⁶ Pb (Ma)
1	0.068	106.35	1263.9	98.68	0.04787±71	0.38726	0.38726	0.10059 (1.76)	0.01524 (0.56)	0.58	97.3±1.7	97.5±0.6	92.9±35
3	0.14	108.71	1336.2	124.6	0.04813±62	0.35653	0.35653	0.10085 (1.42)	0.01519 (0.34)	0.44	97.6±1.4	97.2±0.3	106.0±30
4	0.077	75.69	1281.8	79.08	0.04793±91	0.66831	0.66831	0.08038 (2.45)	0.012163 (0.77)	0.57	78.5±1.9	77.9±0.6	96.1±49

Note. Zircon fractions: 1 – 18 grains, 3 – 35 euhedral grains, 4 – 30 grains.

tization zones in the Early Proterozoic Pezhostrov Island gabbro-anorthosite massif in the Belomorian Mobile Belt in the White Sea area [Sharkov *et al.*, 1994] indicates that zircon recrystallization coupled with a diminish of its grain sizes does not affect the isotopic characteristics of this mineral, and its age evaluated using these grains is close to the age of zircon crystallization from the melt [Zinger *et al.*, 2001]. This led us to believe that the Mesozoic age obtained for zircon from gabbro-norite from the Markov depression corresponds to the crystallization age of this mineral.

[38] Finds of ancient zircon in gabbroids from the axial MAR zone put forth the problem of interpreting the nature of this mineral itself, as to whether it crystallized from a magmatic melt and, hence, its age corresponds to the crystallization age of the rock, or the zircon is a relict and xenogenic mineral that was not decomposed during the melting of the rock. According to currently adopted concepts, the opening of the Central Atlantic started at approximately 170 Ma and continues until now [Pushcharovskii, 2001]. This led Pilot *et al.* [1998] to hypothesize that zircon could be preserved in the mantle at temperatures of about 1000°C for 150 m.y. without losses of its radiogenic lead. These researchers proposed two possible explanations for the nature of ancient zircon in the gabbroids:

[39] (1) The rifting coupled with the opening of the Atlantic resulted in the tectonic disintegration and imbrication of the continental crust, which was broken into a series of tectonic slabs as a consequence of subhorizontal thrusting in the continental lithosphere. Involved in small-cell convection in the upper mantle, these continental lithospheric fragments were remelted. The convection cells that circulated on both sides of the ridge facilitated the displacement of these semi-molten zircon-bearing rocks toward the spreading axis, where they took part in the formation of the gabbroids.

[40] (2) The continental crustal material has been preserved in the Kane zone since the opening of the Atlantic because of the migration of the transform fault and jumps of the ridge axis. Part of this material later subsided in the axial zone of the ridge and was involved in the origin of the gabbroids.

[41] Thus, these researchers believe that the ancient zircon is of continental genesis, is not related to oceanic magma generation, and, hence, cannot provide information on the age of its host rocks. At the same time, geological, petrological, and isotopic-geochemical data provide no evidence that continental material can occur either in the Kane Fracture Zone or in the Markov depression. Moreover, the Fe-Ti-oxide silicic rocks found in the walls of the depression are typical of the third layer of slow-spreading ridges, such as MAR or the Southwest Indian Ridge, and of some ophiolitic associations, such as Monviso in the Western Alps [Lombardo *et al.*, 2002; Rubatto and Gebauer, 2000]. These rocks typically bear zircon with analogous unusual sectorial zoning, which is uncommon in this mineral from continental rocks.

[42] These facts demonstrate that there is no need to propose any specific mechanism for the genesis of the zircon. Furthermore, according to experimental data, zircon can be easily dissolved in basaltic magmas and can crystallize only from melts oversaturated with silica [Watson and Harrison, 1983], and, thus, the occurrence of this mineral in rocks of

the silicic Fe-Ti-oxide association can hardly be accidental. This led us to believe that the zircon crystallized from melts that were emplaced into the oceanic lithosphere, and the zircon age corresponds to the age of its host rocks.

Rock Chemistries

[43] The concentrations of major components in the rocks (Table 10) were determined at the Geological Institute of the Russian Academy of Sciences by conventional techniques. The rocks were analyzed for trace elements at the Department of Mineralogy and Petrology of the University of Granada, Spain. Zr was determined by XRF, using the technique that involves fusing with Li tetraborates (the accuracy of the method is $\pm 5\%$ per 100 ppm Zr). Other trace elements were analyzed by ICP-MS after decomposing 0.1000 g of the powdered material in an $\text{HNO}_3 + \text{HF}$ mixture in a teflon vessel at 180°C and a pressure of 200 pounds per square inch for 30 min and subsequent dissolving in 100 ml of 4% HNO_3 . The accuracy of the analysis was close to $\pm 5\%$ at an analytical concentration of 10 ppm. The results are summarized in Table 11.

[44] Our analyses of the basalts and plutonic rocks from the study area for major and trace elements and for REE indicates that, having many common features, these rocks nevertheless show broadly varying geochemistry. The example of sites I1060 and I1063 demonstrates that samples from a single dredge are characterized by similar fractionation patterns of elements, but these patterns for analogous rocks vary from site to site. This suggests that the dredge captured rock fragments mostly from a single locality but not from the whole dredging course.

Major Elements

[45] As follows from Table 10 and Figure 11, all of the rocks affiliate with the tholeiitic series. The composition points of the basalts and hornblende dolerite lie practically exactly on the boundary line separating the tholeiitic and calc-alkaline series, and sample I1072/1 is closer to MORB. All other rocks can be subdivided into two groups according to their major-element compositions: magnesian and ferrous. The rocks of the first group are primitive gabbroids and troctolites from sites I1032, I1060 (samples 10 and 12), and I1069. They are compositionally close to N-MORB and were, perhaps, produced by such melts. The rocks of the second group are Fe-Ti-oxide gabbro-norites, gabbro-norite-diorites, and diorites from sites I1060 and I1063. They are characterized by high contents of TiO_2 (up to 4.47 wt %) and elevated concentrations of P_2O_5 (up to 1.44 wt % in gabbro-norite I1063/5). It is interesting that the K_2O concentrations of the rocks remain low and reach a maximum of 0.40 wt % in the same gabbrodiorite, whereas this concentration in the trondhjemites is as low as 0.16 wt %. The trondhjemites and harzburgites are quite different and have the lowest contents of these elements.

Table 10. Major-element composition (wt %) of the rocks

Analyt. spots	SiO ₂	TiO ₂	Al ₂ O ₃	Fe ₂ O ₃	FeO	MnO	MgO	CaO	Na ₂ O	K ₂ O	P ₂ O ₅	LOI	Total
I1026/21	49.38	1.69	14.99	4.22	5.29	0.08	8.86	10.28	2.91	0.33	0.19	1.39	99.61
I1027/5	50.67	1.75	14.65	3.30	7.08	0.10	6.92	9.59	2.92	0.46	0.17	1.77	99.38
I1032/7	46.77	0.15	11.78	3.68	5.39	0.09	18.20	9.76	1.38	0.10	0.01	2.53	99.83
I1060/1	47.80	1.23	15.70	1.33	7.08	0.17	8.77	11.30	3.25	0.12	0.15	3.26	100.16
I1060/2	50.20	0.88	15.20	1.88	6.85	0.17	7.67	11.61	3.31	0.12	0.14	1.75	99.78
I1060/10	47.56	0.42	15.23	3.72	5.98	0.19	10.91	12.72	1.77	0.06	0.01	0.89	99.46
I1060/12	52.12	0.31	16.54	2.01	4.79	0.19	10.05	10.06	2.63	0.07	<0.01	1.00	99.77
I1060/18	59.72	1.65	13.04	2.23	8.50	0.15	2.43	5.57	4.92	0.29	0.44	0.80	99.74
I1060/57	77.30	0.23	12.48	0.41	0.63	0.02	0.16	1.68	5.82	0.16	0.02	0.40	99.31
I1063/1	47.38	4.47	12.90	3.82	11.38	0.18	5.78	9.08	3.18	0.10	0.09	1.20	99.56
I1063/2	45.44	0.21	3.28	2.73	7.92	0.16	36.75	1.19	0.42	0.10	0.05	1.30	99.55
I1063/5	47.20	2.98	13.40	5.33	11.65	0.27	4.97	7.62	3.86	0.40	1.44	0.55	99.67
I1063/6	43.99	4.39	14.13	5.24	12.37	0.19	5.02	8.14	3.34	0.27	0.65	1.74	99.47
I1069/16	45.61	0.11	18.65	2.19	2.86	0.11	12.11	14.02	1.35	0.04	<0.01	2.43	99.48
I1071/1	65.50	0.93	14.43	2.90	3.12	0.07	2.33	2.68	5.64	0.14	0.27	2.00	100.01
I1072/1	48.49	1.06	15.86	3.69	7.28	0.17	8.93	11.50	2.55	0.09	0.09	0.37	100.08
L1140/2	48.00	1.28	15.80	1.95	7.16	0.15	9.24	12.13	2.42	0.28	0.11	1.37	99.89

Note. See text for petrographic characteristics of the rocks.

[46] As is seen in Figure 16, all analyses of the rocks can be approximated by a single line, i.e., judging from their major-element compositions, all of these rocks can be regarded as derivatives of a single parental melt like MORB. However, the analysis of the concentrations of trace elements points to a more complicated situation (see below).

Trace and Rare-Earth Elements

[47] The chondrite-normalized REE patterns of the rocks are presented in Figure 17. The basalts and dolerites are characterized by practically unfractionated REE patterns with unclearly pronounced negative Eu anomalies, as is also typical of the cumulate harzburgites (sample I1063/2). In contrast to them, all gabbroids are depleted in LREE and have positive Eu anomalies. The primitive troctolites and gabbro bear the lowest concentrations of REE, particularly LREE, which are close to chondritic ones. The ilmenite-hornblende (Fe-Ti-oxide) varieties of the rocks are notably different from other varieties and have higher REE concentrations, which are close to those in the basalts; but these rocks differ from the basalts in having lower LREE contents and well pronounced positive Eu anomalies. The diorites and granites have REE concentrations by one order of magnitude higher than in the other rocks and generally flat REE patterns with clearly pronounced negative Eu anomalies. Slight LREE enrichment was detected only in the plagiogranites.

[48] The spidergrams of the rocks normalized to the primitive mantle (PM), N-MORB, and E-MORB are only insignificantly different from one another (Figures 18–20) and, thus, are considered collectively. As can be seen from these patterns, the contents of incompatible elements in basalts and

plutonic rocks from site I1063 are the closest to the analogous values of E-MORB, whereas gabbroids from other sites are close to N-MORB. The simplest fractionation patterns of these elements are characteristic of the basalts, and the most complicated ones are typical of the plutonic rocks. As could be expected, the highest concentrations of these elements typically occur in the diorites and granites, interme-

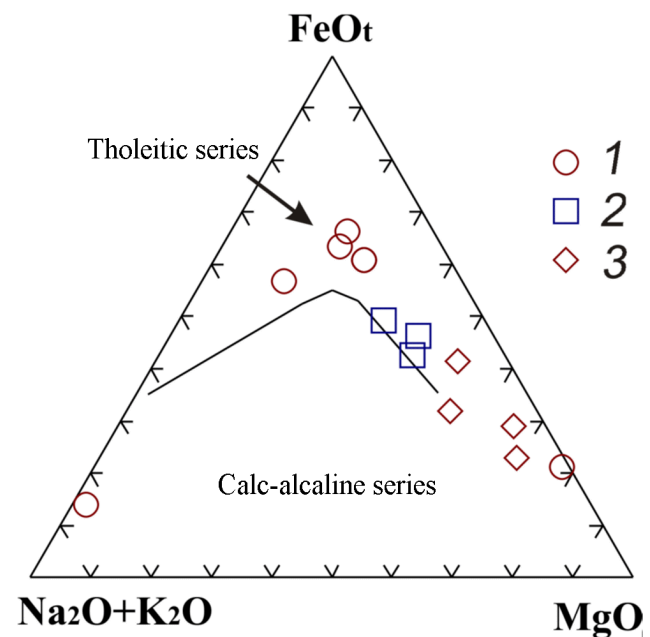


Figure 16. AFM diagram for the compositions of the rocks. 1 – plutonic rocks of silicic Fe-Ti-oxide series; 2 – basalts and dolerites; 3 – primitive troctolites and gabbro.

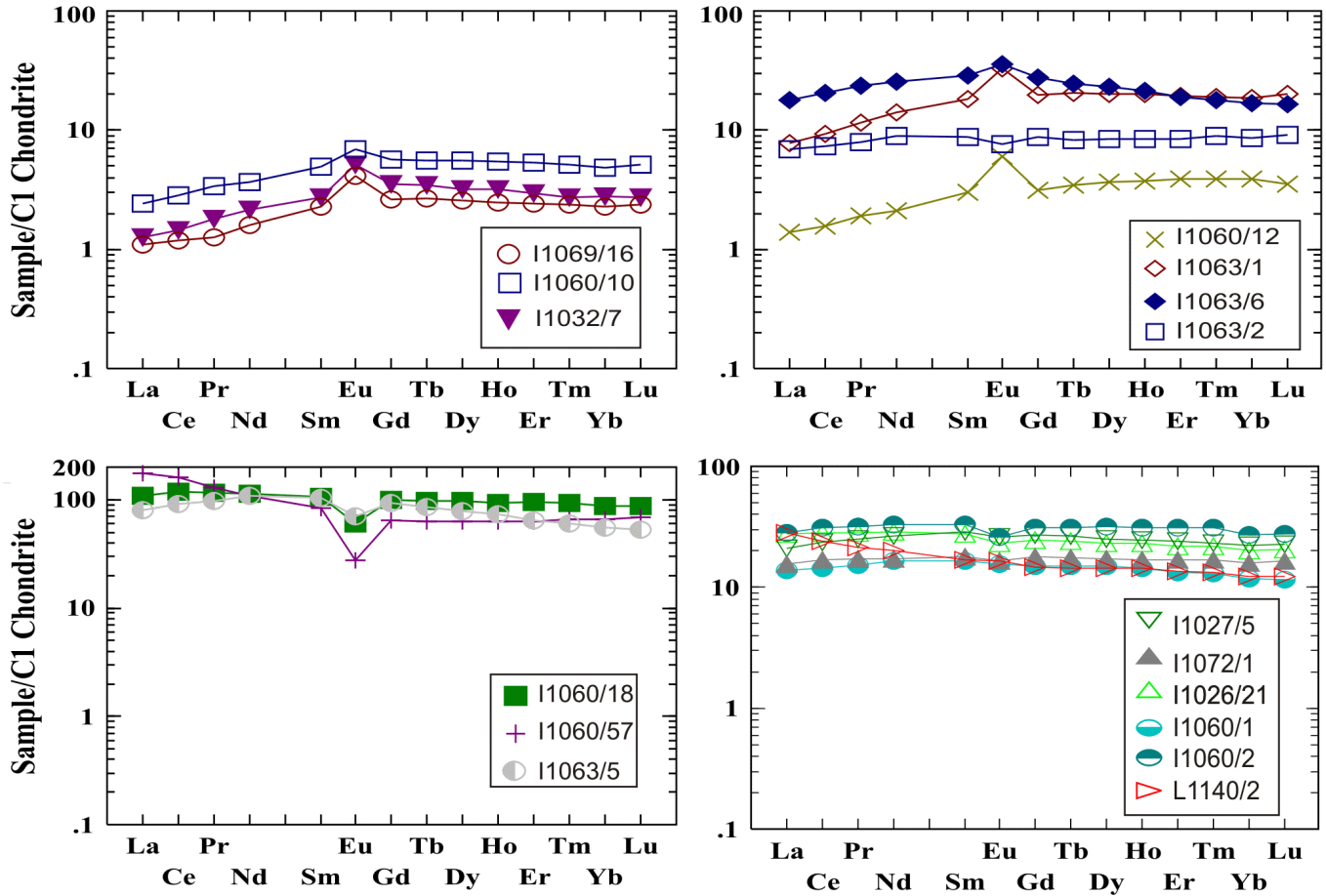


Figure 17. REE patterns of the rocks normalized to C1 chondrite [McDonough and Sun, 1995].

diat values are most common in the Fe-Ti-oxide gabbroids, and the minimum ones were detected in the troctolites and gabbro.

[49] Most of the rocks are characterized by positive Pb anomalies and, often, also U anomalies; the opposite situation is typical only of the diorites, granodiorites, and plagiogranites. Most of the gabbroids have positive Sr and Eu anomalies, whereas the intermediate and acid rocks have negative anomalies at these elements. The only exceptions are the harzburgites, which have negative Sr and Eu anomalies. The overwhelming majority of the rocks is characterized by negative anomalies at Zr, Hf (the only exceptions are basalts I1027/5 and I1026/21), and Th (except only for the granites, which have small positive anomalies). Rocks from site I1063, particularly the Fe-Ti-oxide gabbroids, have strong positive anomalies at Ta and Nb and negative anomalies at Hf. Along with basalts from sites I1026 and I1027, these rocks are characterized by clearly pronounced positive anomalies at Cs and Rb, whereas the diorites and plagiogranites from site I1060 have negative anomalies at Rb.

[50] The concentrations of incompatible elements in our sample of the cumulus harzburgite (sample I1063/2) are generally notably higher than in the primitive mantle (Figure 18) at a generally similar character of fractionation, which is

different from those in other rocks from the same site. These concentrations are only insignificantly lower than in E-MORB (Figure 20). According to the geochemical criteria in [Reverdatto *et al.*, 2005], this harzburgite, which contains 1.35 ppm Sm, 1.64 ppm La, and 1.46 ppm Yb at a sum of REE of more than 20 ppm (Table 11), belongs to peridotites of crustal provenance. It should be stressed that some cumulate ultramafics from this site contain rare grains of kaersutite and ilmenite. This suggests that the ultramafic cumulates are the highest temperature members of the Fe-Ti-oxide association. The assemblages of trace elements contained in these rocks are generally the same as in other derivatives, but their concentrations are much lower.

[51] The ore-element compositions of the samples were normalized to the primitive mantle (Figure 21). Note that none of the rocks, including fresh basalts containing volcanic glass, shows elemental patterns notably different from that of PM. As was mentioned above, all of the rocks are enriched in Pb, with its highest contents detected in basalts I1072/1, Fe-Ti-oxide gabbroids I1063/1 and I1063/6, diorites I1060/18, and trondhjemitites. Practically all of the rocks display positive Ga anomalies. The primitive gabbroids are characterized by negative Sn and Mo anomalies, whereas most of the Fe-Ti-oxide gabbroids and, particularly, the late derivatives

Table 11. Trace-element and REE composition (ppm) of rocks from the Markov depression

Sample	Ba	Rb	Sr	Y	Zr	Nb	Th	Pb	Ga	Zn	Cu	Ni	V
I1026/21	35.648	7.95	177.122	35.196	122.744	7.446	0.497	1.417	17.365	75.177	56.48	134.099	257.98
I1027/5	21.888	7.321	135.835	37.37	111.989	4.71	0.277	1.061	17.754	86.588	69.446	118.475	289.412
I1032/7	46.156	1.306	84.763	4.826	8.111	0.773	0.027	0.555	7.55	37.629	153.402	435.832	111.914
I1060/10	8.125	0.411	98.198	8.552	11.526	0.979	0.043	0.525	13.526	49.439	9.125	128.728	176.38
I1060/12	12.822	0.896	124.083	5.636	6.756	0.747	0.019	0.54	12.801	35.746	54.355	86.251	149.879
I1060/18	76.999	5.259	116.074	155.818	29.531	20.939	1.192	2.208	32.472	117.254	13.484	9.959	38.326
I1060/57	110.01	1.336	69.532	107.77	10.435	23.313	5.231	2.526	26.951	9.345	4.212	6.341	6.41
I1063/1	30.388	2.191	142.374	30.012	49.038	14.38	0.042	0.978	21.501	150.772	69.233	49.506	318.748
I1063/2	12.934	2.897	18.636	13.067	11.177	1.704	0.068	0.577	3.604	78.743	4.347	1786.31	49.543
I1063/5	77.58	11.806	150.814	112.006	30.375	25.437	0.486	1.116	25.11	152.912	39.264	105.781	83.563
I1063/6	39.153	12.96	167.428	32.855	35.647	10.257	0.123	1.282	21.734	147.207	43.94	29.566	218.413
I1069/16	4.857	0.474	99.917	3.811	6.681	0.727	0.027	0.631	8.994	18.473	106.216	361.131	93.917
I1072/1	25.551	1.509	98.771	25.218	57.158	3.488	0.273	1.686	14.25	66.177	96.864	105,781	244,544
I1060/1	13.576	0.916	118.156	22.276	49.61	3.454	0.273	0.740	14.236	69.304	74.017	136.55	227.011
I1060/2	34.573	0.797	91.786	48.466	43.93	6.629	0.258	1.152	15.573	67.611	83.415	77.36	210.981
L1140/2	67.925	3.925	153.492	21.049	63.40	9.820	0.661	0.684	14.089	65.355	74.688	176.26	229.835
Sample	Cr	Hf	Cs	Sc	Ta	Co	Li	Be	U	Sn	Mo	La	Ce
I1026/21	237.341	3.10	0.297	34.809	0.51	39.613	7.079	0.776	0.233	1.209	0.529	6.58	17.35
I1027/5	208.26	3.041	0.246	39.58	0.354	41.12	5.227	0.764	0.145	1.025	0.246	4.93	14.41
I1032/7	473.634	0.25	0.01	28.658	0.031	66.533	7.01	0.149	0.044	0.01	0.01	0.30	0.88
I1060/10	713.353	0.383	0.01	36.943	0.051	40.797	5.837	0.318	0.037	0.05	0.079	0.58	1.74
I1060/12	44.349	0.218	0.01	34.307	0.03	37.352	2.179	0.27	0.05	0.06	0.095	0.33	0.96
I1060/18	21.893	2.416	0.213	25.269	1.649	18.831	1.552	2.895	0.253	7.487	0.162	25.83	72.16
I1060/57	6.041	0.668	0.029	2.787	2.866	2.23	1.123	5.175	0.86	5.462	0.001	41.73	97.36
I1063/1	44.306	1.501	0.117	53.137	1.015	47.796	4.334	0.561	0.029	0.209	0.558	1.84	5.68
I1063/2	3134.9	0.381	0.061	15.352	0.144	93.668	4.136	0.278	0.045	0.01	0.141	1.64	4.53
I1063/5	81.606	1.241	0.049	29.537	1.461	32.291	3.63	1.288	0.131	2.374	1.187	19.02	56.09
I1063/6	24.283	1.11	0.168	37.446	0.733	43.382	4.064	0.581	0.052	0.479	0.448	4.27	12.45
I1069/16	2574.48	0.201	0.01	24.892	0.035	34.229	1.592	0.187	0.028	0.01	0.041	0.26	0.73
I1072/1	273.673	1.739	0.01	38.073	0.324	41.12	0.886	0.538	0.111	0.69	0.338	3.67	10.32
I1060/1	351.699	1.465	0.157	34.577	0.295	38.577	3.852	0.574	0.041	1.019	0.368	3.294	8.852
I1060/2	224.269	1.461	0.103	34.878	0.432	37.516	3.442	1.022	0.007	1.461	0.501	6.636	18.999
L1140/2	357.079	1.724	0.186	36.083	0.659	41.936	4.482	0.451	0.196	0.965	0.778	6.732	14.65
Sample	Pr	Nd	Sm	Eu	Gd	Tb	Dy	Ho	Er	Yb	Tm	Lu	
I1026/21	2.65	13.40	4.19	1.35	5.06	0.90	5.84	1.30	3.61	3.43	0.55	0.52	
I1027/5	2.39	12.31	4.36	1.50	5.53	1.00	6.37	1.38	3.99	3.79	0.59	0.57	
I1032/7	0.17	1.00	0.42	0.30	0.72	0.13	0.82	0.18	0.49	0.47	0.07	0.07	
I1060/10	0.32	1.72	0.76	0.40	1.17	0.21	1.42	0.31	0.88	0.83	0.13	0.13	
I1060/12	0.18	0.99	0.46	0.35	0.65	0.13	0.93	0.21	0.64	0.66	0.10	0.09	
I1060/18	11.00	53.12	16.13	3.52	20.63	3.62	24.52	5.33	15.59	14.99	2.38	2.24	
I1060/57	12.38	50.60	12.82	1.61	13.19	2.38	16.00	3.55	10.37	11.16	1.68	1.75	
I1063/1	1.10	6.55	2.79	1.92	4.07	0.76	5.08	1.14	3.20	3.17	0.48	0.51	
I1063/2	0.75	4.16	1.35	0.44	1.79	0.31	2.13	0.48	1.39	1.46	0.23	0.23	
I1063/5	9.30	50.29	15.95	4.11	19.04	3.16	19.70	4.11	10.67	9.39	1.54	1.33	
I1063/6	2.22	11.83	4.37	2.06	5.64	0.91	5.82	1.21	3.16	2.87	0.46	0.42	
I1069/16	0.12	0.74	0.35	0.24	0.54	0.10	0.65	0.14	0.40	0.39	0.06	0.06	
I1072/1	1.62	8.00	2.74	0.96	3.64	0.66	4.35	0.96	2.78	2.69	0.43	0.42	
I1060/1	1.45	7.64	2.54	0.90	3.07	0.55	3.81	0.82	2.21	1.99	0.33	0.29	
I1060/2	3.04	15.54	5.03	1.50	6.38	1.16	8.07	1.76	5.13	4.63	0.78	0.69	
L1140/2	2.03	9.37	2.57	1.00	3.04	0.54	3.65	0.82	2.22	2.07	0.34	0.31	

Table 11. Continued)

Sample	Pr	Nd	Sm	Eu	Gd	Tb	Dy	Ho	Er	Yb	Tm	Lu
I1026/21	2.65	13.40	4.19	1.35	5.06	0.90	5.84	1.30	3.61	3.43	0.55	0.52
I1027/5	2.39	12.31	4.36	1.50	5.53	1.00	6.37	1.38	3.99	3.79	0.59	0.57
I1032/7	0.17	1.00	0.42	0.30	0.72	0.13	0.82	0.18	0.49	0.47	0.07	0.07
I1060/10	0.32	1.72	0.76	0.40	1.17	0.21	1.42	0.31	0.88	0.83	0.13	0.13
I1060/12	0.18	0.99	0.46	0.35	0.65	0.13	0.93	0.21	0.64	0.66	0.10	0.09
I1060/18	11.00	53.12	16.13	3.52	20.63	3.62	24.52	5.33	15.59	14.99	2.38	2.24
I1060/57	12.38	50.60	12.82	1.61	13.19	2.38	16.00	3.55	10.37	11.16	1.68	1.75
I1063/1	1.10	6.55	2.79	1.92	4.07	0.76	5.08	1.14	3.20	3.17	0.48	0.51
I1063/2	0.75	4.16	1.35	0.44	1.79	0.31	2.13	0.48	1.39	1.46	0.23	0.23
I1063/5	9.30	50.29	15.95	4.11	19.04	3.16	19.70	4.11	10.67	9.39	1.54	1.33
I1063/6	2.22	11.83	4.37	2.06	5.64	0.91	5.82	1.21	3.16	2.87	0.46	0.42
I1069/16	0.12	0.74	0.35	0.24	0.54	0.10	0.65	0.14	0.40	0.39	0.06	0.06
I1072/1	1.62	8.00	2.74	0.96	3.64	0.66	4.35	0.96	2.78	2.69	0.43	0.42
I1060/1	1.45	7.64	2.54	0.90	3.07	0.55	3.81	0.82	2.21	1.99	0.33	0.29
I1060/2	3.04	15.54	5.03	1.50	6.38	1.16	8.07	1.76	5.13	4.63	0.78	0.69
L1140/2	2.03	9.37	2.57	1.00	3.04	0.54	3.65	0.82	2.22	2.07	0.34	0.31

have positive anomalies at these elements. Analogous patterns are also shown by the basalts, whose concentrations are nearly normal. The Li contents of the rocks are close to or higher than those in PM. This also pertains to the basalts and peridotites. Moreover, the peridotite is enriched in Mo and Pb and depleted in Cu, Sn, and, to a lesser degree, V compared to PM.

[52] Most of the rocks, except only the late derivatives and coarse-grained gabbro I1060/10, display positive Cu anomalies. Rocks from site I1060, particularly the trondhjemites, are depleted in Cu, whereas rocks from site I1063 (except sample I1063/6) are, conversely, slightly enriched in this element. All of the basalts are characterized by elevated contents of Cu, whose highest concentrations were detected in olivine gabbro from site I1032 and troctolites from site I1069. The Zn concentrations are generally higher than the normal value, particularly in the Fe-Ti-oxide gabbroids. Most of the samples display a negative correlation between their Cu and Zn concentrations.

[53] Similarly to the trace-element spidergrams of the primitive gabbroids and rocks of the Fe-Ti-oxide association, the configurations of ore-element plots of these rocks are also notably different. This pertains, first of all, to the Sn and Mo concentrations, which are notably higher in the latter rocks at low Ni and, particularly, Cr concentrations. The ore-element plots for the basalts are, again, much closer to the plots of rocks of the Fe-Ti-oxide association than to those of the primitive troctolites and gabbroids. Along with elevated concentrations of Cs and Pb in these rocks, this suggests that these rocks were produced by the mixing of two magma types or were derivatives of the magmas of the second association.

[54] Thus, the geochemistry of the seafloor rocks from the Sierra Leone MAR segment indicates that practically all of them, except only the diorites and trondhjemites, are en-

riched in Pb, U, Rb, Ta, Nb, Cs, and Rb relative to the primitive mantle and are depleted in Zr, Th, and Hf. The minimum concentrations of incompatible elements are typical of the primitive troctolites and gabbro, intermediate contents were detected in the hornblende Fe-Ti-oxide gabbronorites, and the maximum ones occur in the diorites and plagiogranites. Only some of the anomalies, such as those at Sr and Eu, were obviously controlled by crystallization differentiation, whereas this is not as evident for other elements: the rocks can be either depleted or enriched in components mobile in aqueous fluids. This also pertains to the peridotite with a relict cumulate texture.

[55] **Spreading versus plume association.** According to REE ratios, many researchers classify MAR basalts with two types of associations: related to spreading (normal) or plume (anomalous) [Dmitriev *et al.*, 1999; Douglass *et al.*, 1999; Schilling *et al.*, 1983; Silant'ev *et al.*, 2002]. Following Schilling *et al.* [1983], the distinction is commonly drawn using the $(La/Sm)_N$ and $(Ce/Yb)_N$ ratios. According to their $(La/Sm)_N$ ratio equal to 0.70–0.83, all samples of the basalts and dolerites plot near the boundary between the plume and spreading associations. Although this systematics was proposed for basalts, we also applied it to the intrusive rocks, because their geochemistry retains many features of the parental melts. All of the gabbroids, including their Fe-Ti-oxide varieties plot within the field of normal (spreading) associations $(La/Sm)_N < 0.7$. The diorites belong to intermediate varieties with $(La/Sm)_N = 0.74$ and 0.99, and the trondhjemites have this ratio equal to 2.01 (if this criterion is applicable to them) and fall into the field of plume associations. The $(Ce/Yb)_N$ ratios of the trondhjemites is at a maximum and reaches 2.22. $(Ce/Yb)_N$ ratios intermediate between those of these rocks and gabbroids are typical of the diorites, and the gabbroids are characterized by the

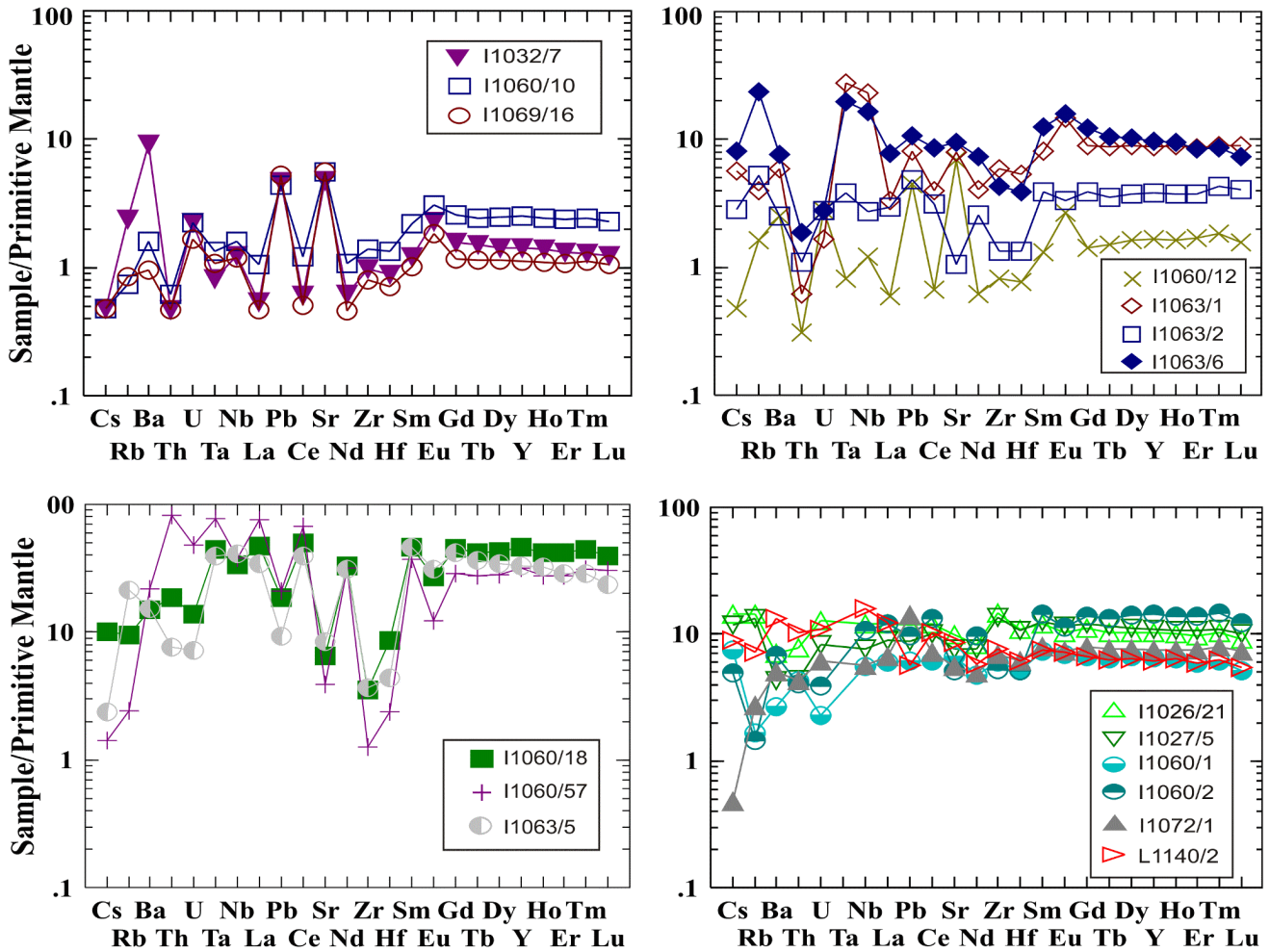


Figure 18. Trace-element composition of the rocks normalized to the primitive mantle [McDonough and Sun, 1995].

minimum values (similarly to the $(\text{Ce}/\text{Yb})_N$ ratio). As in the previous case, the harzburgites and basalts also exhibit intermediate values of this ratio.

[56] It follows that, according to their geochemistry, these rocks should be attributed to the spreading association. The diorites and trondhjemites are the closest to the plume association, although this is hardly significant because these associations are distinguished using basalts but not late derivatives. The rocks most different from the plume association are the gabbroids, including those belonging to the individual group of Fe-Ti-oxide gabbronorites, in spite of their anomalously high concentrations of Ti, Ta, and Nb, as is typical of plume-related melts. The basalts are somewhat different and are characterized, in contrast to the gabbroids, by flat chondrite-normalized REE patterns without significant depletion in LREE. However, these basalts are also heterogeneous: these rocks from sites I1026 and I1027 have positive Rb and, particularly, Cs anomalies, whereas basalt I1072/1 displays negative Rb and Cs anomalies.

[57] Our materials indicate that the rocks include no varieties that can be related (on the strength of geochemical

evidence) to within-plate magmatism. The presence of weak positive Eu anomalies in the basalts suggests that they are not primary partial melts but underwent differentiation in intermediate chambers, in which cumulates of gabbro composition precipitated from the parental melt. An analogous negative anomaly in the diorites and granites suggests that they are late derivatives of the melts during the solidification of these chambers (intrusions). The virtually flat configurations of the HREE patterns indicate that the magmas were generated at moderate depths, and their petrogenesis did not involve garnet.

Discussion

[58] **The general characteristics of rocks of the silicic Fe-Ti-oxide association.** The petrography and geochemistry of the rocks indicate that they probably comprise two groups of plutonic rocks: (i) magnesian (primitive) troctolites, gabbro, and olivine gabbro, whose geochemistry

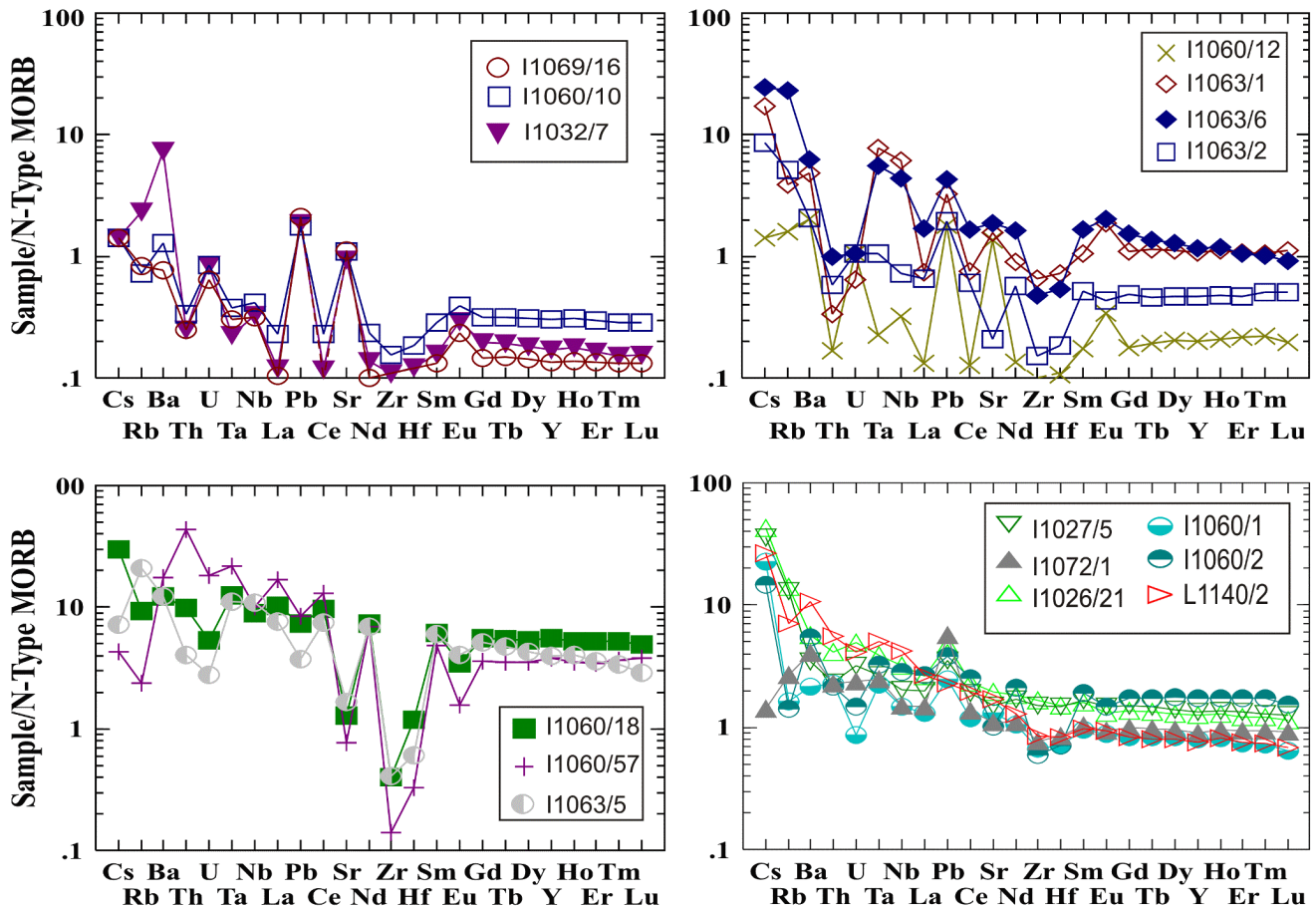


Figure 19. Trace-element composition of the rocks normalized to the N-MORB [Sun and McDonough, 1989].

is close to that of MORB; and (ii) variable kaersutite-bearing Fe-Ti-oxide rocks, including diorites and trondhjemites, which show some characteristics close to those of E-MORB but notably differ from them in having a deficit in LREE, Zr, Th, Hf, K, and, sometimes, Ba. A separate group is composed of the basalts, which generally have trace-element compositions close to those of MORB but have positive Pb anomalies and, in four samples, also positive Cs and Rb anomalies. The U-Pb zircon of a sample of one of these rocks (cataclased hornblende gabbronorite, sample I1028/1) is 97.42 ± 0.13 Ma (see above). [Sharkov et al., 2004a].

[59] It was mentioned above that most rocks of the Fe-Ti-oxide association in slow-spreading mid-oceanic ridges are thought to have been produced by the fractional crystallization of MORB-type melts [Dick et al., 1992]. However, these rocks notably differ from the final products of the crystallization differentiation of tholeiitic basalts, which are thoroughly studied in continental layered intrusions. The ore mineral of these rocks is titanomagnetite, and they contain practically no magmatic hornblende but bear orthoclase and are typically enriched in trace elements, particularly LREE [Wager and Brown, 1968]. The interpretation of the Fe-Ti-oxide rocks as late derivatives of MORB is also at variance with

their wide occurrence in the Sierra Leone MAR segment in the form of plutonic, subvolcanic, and volcanic rocks.

[60] Furthermore, the petrology and geochemistry of the Fe-Ti-oxide rocks cannot be described within the framework of any currently existing systematics. Although these rocks are often anomalously rich in Ti, Nb, and Ta, as is typical of within-plate melts related to the activity of deep mantle plumes, they are poor in incompatible elements, including LREE. These rocks are characterized by the presence of orthopyroxene, pigeonite-augite, and magmatic hornblende, i.e., minerals typical of the calc-alkaline series, which were produced by melts saturated with silica and water. Elevated water contents in the melts also follow from the separate crystallization of their Fe-Ti oxides (see above). In other words, the petrography and geochemistry of these rocks indicate that they compose a separate magmatic association, which differs from both within-plate rocks and those of the calc-alkaline series but displays certain features of both.

[61] The possibility of the occurrence of such magmas in oceanic environments follows from data obtained by studying melt inclusions in chromite from the dunites of the transitional zone between mantle harzburgites and crustal cumulates in the Oman ophiolitic association [Schiano et

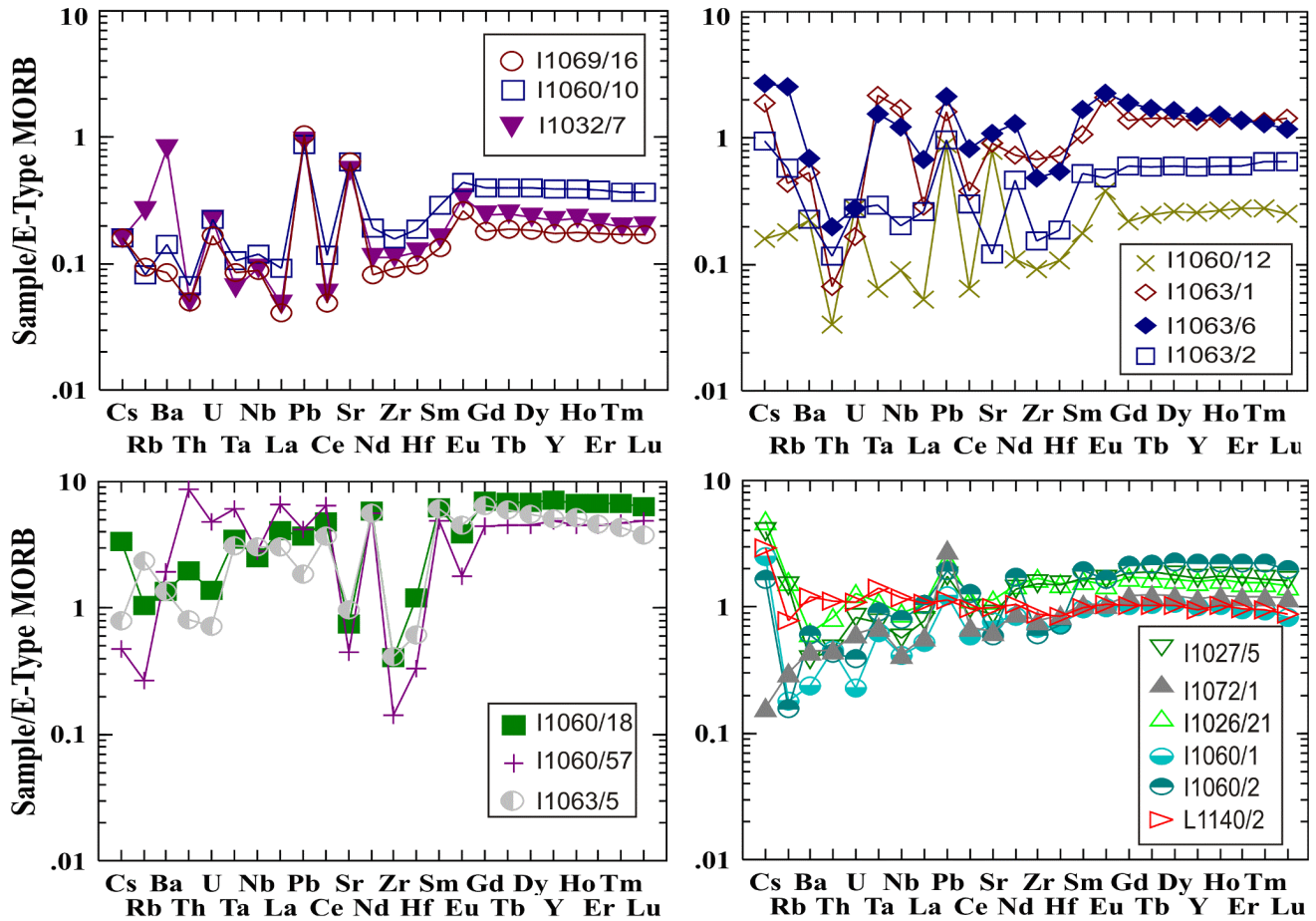


Figure 20. Trace-element composition of the rocks normalized to the E-MORB [Sun and McDonough, 1989].

al., 1997]. The inclusions have a composition of magnesian ($mg\# = 63.5\text{--}66.8$) hypersthene-normative basalt and show depleted REE patterns with significant Nb anomalies, as is typical of melts of suprasubduction provenance, but, in contrast to the latter, high TiO_2 concentrations (of about 3 wt %).

[62] Closely related to the Fe-Ti-oxide association are ultramafic cumulates (harzburgites and lherzolites). As was demonstrated above, these ultramafic rocks display geochemical characteristics notably different from those of mantle rocks, and their mineralogy suggest the presence of at least two independent mineral assemblages. The earlier of them includes Fe- and Ti-rich spinel, which makes it notably different from mantle peridotites through which basaltic melts percolated (the latter rocks show the opposite relations [Piccardo et al., 2004]). Moreover, the rocks dredged at sites within the Sierra Leone MAR segment (sites I1022, I1025, I1032, I1060, I1063, I0168, L1122, and others) include, along with these rocks, also norites, gabbro-norites, olivine norites, *Opx*-bearing troctolites, and bronzitites. All of these features suggest that the area includes a series of intrusive rocks (cumulates) all of which contain low-Ca pyroxene and, often, also magmatic amphibole and Fe-Ti ox-

ides. We propose that this group of intrusive rocks, whose composition varies from ultramafic to acid, should be recognized as an individual silicic Fe-Ti-oxide series. Its sub-volcanic analogues seem to be the ilmenite-hornblende dolerites, and volcanic counterparts are the aphyric Fe-Ti-oxide and plagioclase- and olivine-plagioclase-phyric basalts with abundant disseminated ilmenite, which were dredged at these sites.

[63] The positive Eu and Sr anomalies in the gabbroids of the Fe-Ti-oxide series and negative anomalies in its intermediate-acid members suggest that these elements were fractionated during plagioclase crystallization. Analogous but weaker anomalies of opposite character are also typical of U and Pb, whereas Th, conversely, is enriched in the intermediate-acid rocks. This suggests that the Fe-Ti-oxide gabbro, diorites, and trondhjemites are indeed derivatives of melts other than MORB. As was mentioned above, the rocks of this series and their supposed derivatives plot in classification diagrams within a separate field and but not within the fields of any other known series.

[64] For the equatorial MAR segment, the occurrence of glasses whose Nd-Sr-Pb systematics testify that they were produced by the mixing of isotopically distinct mantle

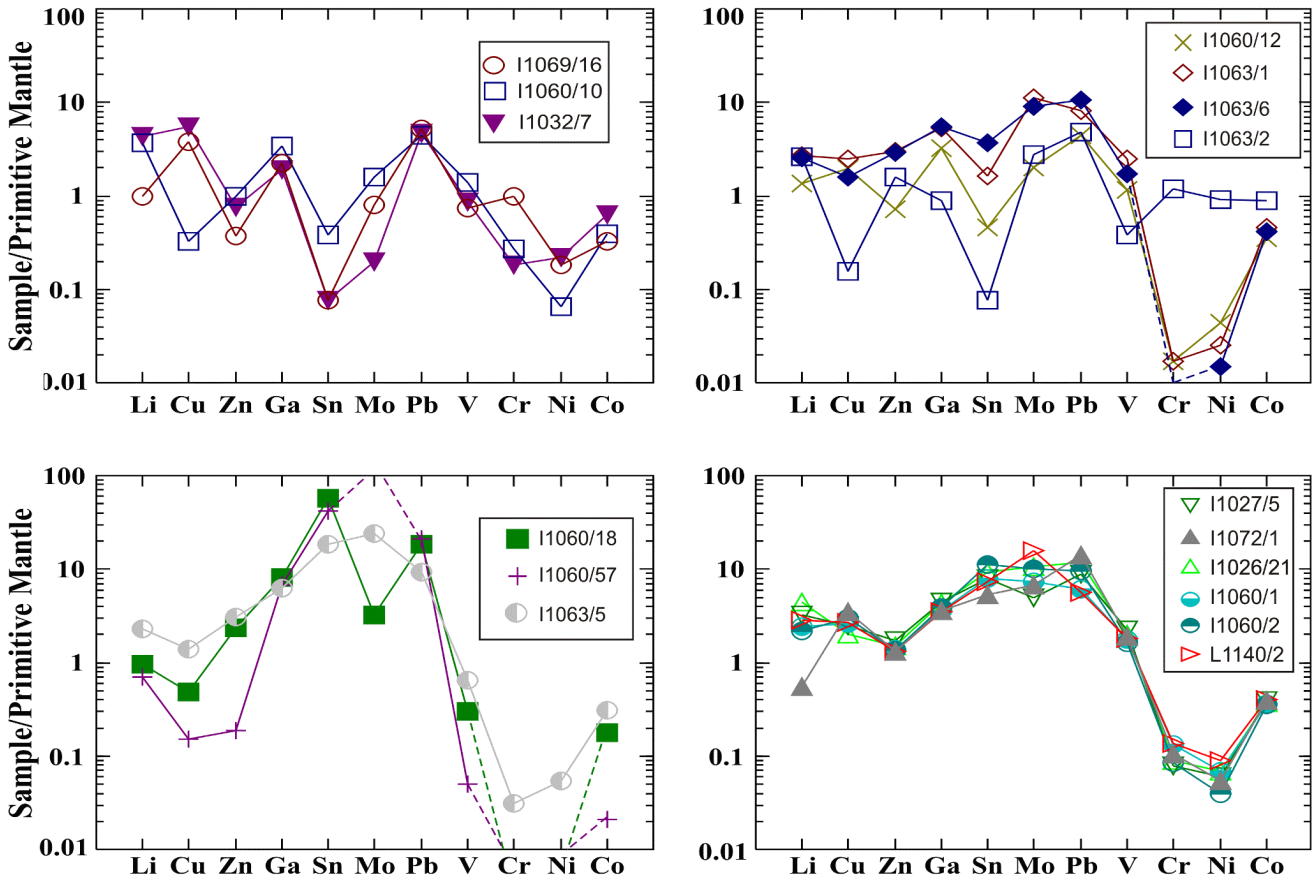


Figure 21. Ore-element composition of the rocks normalized to the primitive mantle [McDonough and Sun, 1995].

sources: HIMU (i.e., that containing excess radiogenic Pb, supposedly related to a subduction component [Zindler and Hart, 1986]) and the depleted mantle: was first suggested by Schilling *et al.* [1994]. These researchers explained this phenomenon by the effect of the hypothetical Sierra Leone plume, which should have partly assimilated the buried subducted material. A complex composition of the melt sources beneath this MAR segment also follows from geochemical data, which point to the existence of three or four mantle reservoirs [Hannigan *et al.*, 2001]. This is in general agreement with our results, according to which the area includes at least two geochemical types of ancient plutonic rocks, and a third one is represented by fresh basalts that are close to E-MORB but show some characteristics distinct from them. At the same time, no magmatic rocks ever found in the area can be related to the activity of plumes, neither are there any traces of subduction, and the characteristics of the silicic Fe-Ti-oxide association are at variance with its affiliation with any of the currently known magmatic series.

[65] The conclusion that such rocks have an unusual genesis was arrived at by Benoit *et al.* [1999] based on studying gabbro cumulates in the Oman ophiolites, and by Holm [2002], who examined the Sr-Nd-Pb systematics of Fe-Ti-oxide gabbro and diorites that occur as dikes in the

Southwest Indian Ridge (Atlantis II Deep, Hole 735 B, ODP Leg 176). According to these geologists, melts of this type have a complicated genesis, including the mixing of MORB-type magmas and LREE-depleted melts.

[66] **The magmas of the silicic Fe-Ti-oxide association as hydrous melts.** The facts that these rocks ubiquitously contain magmatic hornblende and are characterized by the separate crystallization of magnetite and ilmenite serve as direct evidence that the melts contained water. Judging from the Nd-Sr isotopic data, this water was of marine provenance [Sharkov *et al.*, 2004]. This puts forth the question as to how seawater could be brought into the magma-generating region or the already-solid intrusive chamber where crystallization differentiation took place. Water could hardly percolate into it, because heated water or a vapor-water mixture should have ascended along fractures in the host rocks (as is commonly observed in modern volcanic areas) and give rise to various fumaroles in continental environments and to a diversity of black smokers in the ocean. Relations between magmatic melts and water can be vividly illustrated by the example of pillow lavas that were erupted on the seafloor: their chill glasses contain practically no seawater [Simonov *et al.*, 1999], and the

basalts themselves were altered only locally along contraction cracks or in the course of halmyrolysis.

[67] We believe that seawater was brought into the magmatic melt mostly during the process of magma generation, due to the remelting of hydrated mafic-ultramafic rocks in the upper oceanic lithosphere. As was mentioned above, these ultramafic rocks are commonly serpentinized and the gabbroids are variably altered with the development of fibrous actinolite, veins of chlorite, prehnite, epidote, and numerous hydrothermal-metasomatic zones of variable thickness. The LOI values (mostly, the water losses) in the chemical analyses of the gabbroids vary from 1 wt % to 2.5 wt % (Table 8), whereas the analogous values for their serpentinized analogues are as high as 9–17 wt % at average values of 13–14 wt % [Simonov *et al.*, 1999]. When a hot mantle diapir (lithospheric plume) intrudes such hydrated lithospheric material, it is reasonable to expect that this material starts melting, because the presence of water in the rocks notably decreases their solidus temperatures. These magmas of new generation should obviously have some specific geochemical characteristics, which distinguish them from melts that came directly from the mantle, because the composition of these newly formed melts was notably affected by the fractionation of elements during melting and crystallization in the presence of an aqueous fluid.

[68] **Geochemical aspects of the melting of the hydrated oceanic lithosphere.** These aspects are now actively explored in the context of the genesis of the calc-alkaline series via the melting of subducted slabs that consist mostly of MORB-type protoliths. As follows from experimental data, the partial melting of these water-saturated basalts is possible at temperatures higher than 750°C [Peacock *et al.*, 1994]. According to the experimental data in ([Tatsumi *et al.*, 1986], these partial melts should have had high concentrations of Ti, Nb, and Ta. The data presented in [Schiano *et al.*, 1995] suggest that these melts should also have been enriched in silica. This is in good agreement with our petrographic and geochemical data on the rocks of the silicic Fe-Ti-oxide series. Although these rocks are notably different from suprasubduction rocks of the arc calc-alkaline series, they display certain similarities with them, which are caused by the role of water in the genesis of the parental melts.

[69] Important information on the behavior of trace elements during the dehydration of the oceanic crust in subduction zones was obtained by Becker *et al.* [2000] for temperatures of 600–900°C, at which hydrated basites are melted [Peacock *et al.*, 1994]. These researchers have demonstrated that the elements most significantly removed from the protolith are Pb and U, which are followed by Nb, K, Rb, Ba, and, then, by Cs and Sr. An analogous situation exists with serpentinites. The experimental data on trace elements in fluids released from these rocks during deserpentinization indicate that these fluids are enriched in Cs, Be, Li, Cl, As, Sr, Rb, Ba, and Pb, which were borrowed by serpentinites from seawater when the peridotites were altered at the seafloor [Tenthorey and Hermann, 2004].

[70] All of these elements mobile during melting in fluids should have obviously dissolved in the melt and caused the

respective positive anomalies in it relative to MORB. The newly generated melts were not significantly enriched in K likely because of the very low concentrations of this element in the source material (serpentinites, primitive gabbroids, and troctolite; see above). In the course of hydration, Nd, Sm, Zr, and Y are practically immobile, and, thus, their concentrations in the melt did not notably change compared with those in the protolith. Most REE were also not fractionated in the course of this process, because the character of their distribution in rocks remains the same as in MORB, although their total contents notably increased, particularly in the diorites and trondhjemites. The deficit in LREE seen in the chondrite-normalized patterns of the latter two rocks is notably lower (Figure 17), which suggests that these rocks were generated by crystallization differentiation.

[71] In this context, it is worth mentioning that practically all of our samples of the basalts show positive Pb anomalies, and basalts from sites I1026 and I1027 additionally have Cs and Rb anomalies. Conceivably, these basalts underwent mixing with partial melts derived from the hydrated mafic rocks or are themselves basalts of the second generation.

[72] This mechanism of magma derivation related to the remelting of mafic and ultramafic rocks of the hydrated oceanic lithosphere and the associated extraction of more ancient Pb from these rocks provides a plausible clue to understanding the HIMU isotopic source, which was identified MAR. In this situation, there is obviously no need to conjure some hypothetical subduction material to interpret data on the melt sources in these specific active magmatic structures.

[73] The occurrence of cumulus ultramafic rocks among the rocks of the Fe-Ti-oxide association suggests that melting affected not only the altered mafic rocks of the oceanic crust but also serpentinites that developed after ultramafics in the upper oceanic lithospheric mantle. Experimental data indicate that the melting of these rocks at 1–3 kbar (i.e., at depths of 3–10.5 km) can begin already at temperatures of about 930–980°C [Kushiro *et al.*, 1968]. At pressures of about 10–12 kbar and 12 wt % H₂O, the melting temperatures of serpentinites increase to approximately 1115°C. Because of the increase in the Si/(Mg + Fe) ratio, the newly formed melts are quartz-normative [Gaetani and Grove, 1998]. This implies that the solidus temperatures of the serpentinites were significantly lower than the asthenospheric mantle temperatures throughout the whose range of depths possible under these conditions.

[74] Inasmuch as the newly formed melts were in equilibrium with normative olivine and pyroxenes, their first cumulates should have been of ultramafic composition. As follows from experimental data on the *Fo-Di*-SiO₂ system [Kushiro, 1969], which describes the crystallization of such melts, their evolutionary trend should shift (due to the presence of water) toward SiO₂ and result in a granitic liquid as the final derivative.

[75] Available petrological and geochemical data provide evidence that the melts of the silicic Fe-Ti-oxide series could be generated by the remelting of the hydrated oceanic lithosphere, since they are oceanic analogues of mantle-crustal melts. Because of this, these melts share some characteristics with the calc-alkaline series but differ from it in having strongly subordinate amounts of rocks of intermediate and

acid composition, which are predominant in arc series. These differences are obviously caused by the fact that the subducted slabs contain much sediments and continental crustal material from the backarc space [Sharkov, 2003b; Wilson, 1989], which are absent from mid-oceanic ridges. The geochemical differences are no less important: our rocks are generally poor in incompatible elements and have elevated to high concentrations of Fe, Ti, Ta, and Nb, which are atypical of calc-alkaline magmas. Obviously, the latter feature is related to the derivation of the magmas from the rocks of the subducted slab under high pressures, when the residue contains rutile, the main concentrator of Ti, Ta, and Nb [Peacock et al., 1994].

[76] **Possible mechanism forming secondary magmatic systems in the hydrated oceanic lithosphere.** What could cause the processes of melting in this lithosphere? Obviously, this could be only the emplacement of new plumes. Geochemical data indicate that these could not be deep plumes like those maintaining the development of oceanic islands. Available data indicate that the composition of these plumes was most probably close to the MORB source, i.e., they were protuberances on the surface of large asthenospheric lenses beneath mid-oceanic ridges. According to geophysical evidence, such lenses have thicknesses of about 300 km, which makes it possible to maintain the activity of these global structures [Fowler, 2004].

[77] In papers dealing with the possibility of melting of the hydrated oceanic lithosphere during the emplacement of mantle diapirs, it is usually assumed that this melting occurs at contacts with these diapirs [Benoit et al., 1999; Ross and Elthon, 1996]. This is, however, hardly possible because (i) the marginal parts of diapirs (plumes) are cooled in contact with the colder host rocks, and (ii) the mechanism of conductive heat transfer is extremely inefficient and cannot maintain the stable development of magmatic systems. In this sense, a much more promising mechanism is melting above large magma chambers that develop immediately at the plume roof and make it possible underplating, a process responsible for the formation of the lower mafic crust of continents [Rudnick, 1990].

[78] The most probable mechanism that can enable this process is zone melting, which was proved efficient for the formation of the melts of the Paleoproterozoic silicic high-Mg series [Sharkov et al., 1997]. In essence, this process is the ascent of a chamber of a high-temperature mantle magma through the mafic lower crust by means of melting its roof rocks and the simultaneous crystallization of the melt near the chamber bottom because of the difference between the adiabatic gradients and melting points [Sharkov, 1980]. Since the temperature of the parental mantle magmas of the MORB type is 1260–1280°C [Sobolev et al., 1988] or are even as high as 1300–1400°C [Ryabchikov, 2003], i.e., much higher (by at least 300–400°C) than the solidus temperature of serpentinites and hydrated mafic rocks (see above), this heat is sufficient to induce the melting of the roof rocks.

[79] The ascent of such a new plume should have stopped when it reached the limit of its buoyancy in the low-density serpentinitized upper mantle. After this, the plume heads started spreading laterally. This process was associated with

adiabatic decompression and the melting of the ultramafic plume material. The newly formed melt first accumulated underneath the cooled roof of the plume and then migrated upward along arrays of extension fractures and formed large mantle chambers. Data on ophiolitic associations indicate that such a chamber originally developed between the plume head and the overlying older lithosphere [Sharkov et al., 2001]. Due to convection, heat was lost from this chamber predominantly through its roof, which, in turn, should have inevitably brought about its melting because of the relatively low solidus temperatures of the hydrated roof rocks. The relatively cold and partly molten material of the roof should have sunk to the inner parts of the chamber or has completely or partly dissolved in the melt (Figure 22). This dissolution seems to have not always been complete, as follows from the occurrence of foreign assemblages among the minerals (see above). The structural water of the hydroxyl-bearing minerals in the melting rocks should have been actively consumed by the melt and maintain its elevated water contents.

[80] In contrast to solidification processes, which proceed from cold contacts toward the central portion of cooling magmatic chambers (intrusions) that are isolated from the host rocks by marginal zones [Sharkov, 1980; Wager and Brown, 1968], the processes of melting should have proceeded in the opposite direction (from the center outward). Because of this, the melt received components not only from the melting roof rocks of the chamber but also from rocks in its periphery, as well as fluid components from the strongly heated rocks in the remote periphery. This likely predetermined the unusual features of these melts, their enrichment in components most mobile under these conditions, such as silica, Ti, Pb, and Cu.

[81] According to the mechanism of zone melting, the melting of the roof should be associated with the crystallization of the most refractory minerals near the chamber bottom. This mechanism maintains the continuous ascent of the chamber through the lithosphere and the systematic involvement of progressively higher lithospheric levels (including layer 3 of the oceanic crust) in the melting process. The long-lasting character of this process should have been maintained by the periodic arrival of new portions of fresh melt from the mantle magma-generating zone, as was established, for example, for the Paleoproterozoic [Sharkov, 2003a]. The surmised inner structure of such a magmatic system is illustrated in Figure 23.

[82] The ascent of the magma chamber and the associated large-scale assimilation of the material of the overlying lithosphere resulted in the continuous enrichment of the melt in the melting products of this lithosphere and in the products of crystallization differentiation. Inasmuch as the melt composition in the chamber was constantly equalized by convection (which homogenized the whole melt volume), these changes should also have affected the composition of the crystalline phases settling near the chamber bottom. Consequently, the ascending chamber left behind a trail in the form of a series of specific cumulates, ranging from ultramafic to mafic rocks, with the inner structure of the series resembling that of layered intrusions. Indeed, as was mentioned above, MAK acoustic sounding data indicate that

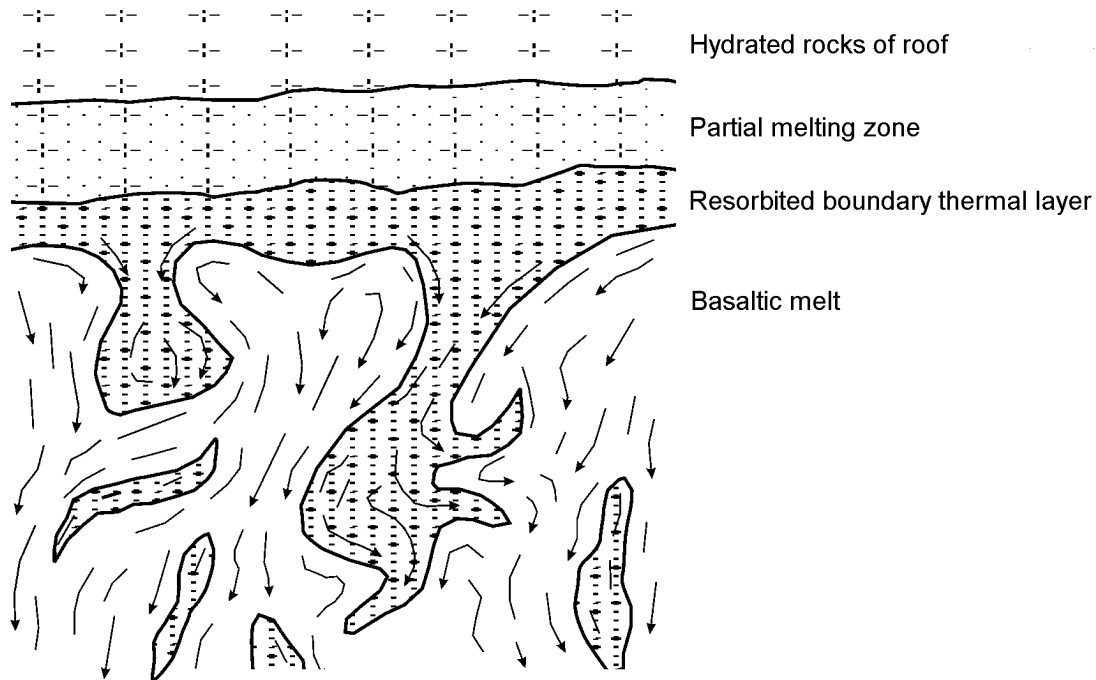


Figure 22. Scheme illustrating the melting of the magma chamber roof beneath the seafloor.

the flanks of the Markov depression look like a cross section through a large layered intrusion. Low-melting components should have enriched the stirred layer of the melt and produced Fe-Ti-oxide rocks and trondhjemites late in the evolutionary course of such a magmatic system.

[83] Unlike typical layered intrusions, this mechanism of the origin of the layered series implies that the cumulate and the crystallization products of the melt could include the disintegrated incompletely melted material of the ancient continental lithosphere, which consisted of various mafic and ultramafic rocks. The U-Pb age of the latter could be as old as hundreds of million years [Pilot *et al.*, 1998; Sharkov *et al.*, 2004b]. This suggests that the third layer of the MAR oceanic crust was formed for a long time and is heterogeneous due to the multiple emplacements of asthenospheric plumes into the oceanic lithosphere. When this lithosphere was not hydrated, it gave rise to melts of the MORB type, and, conversely, the silicic Fe-Ti-oxide series was derived from the lithosphere affected by low-temperature alterations.

[84] A portion of melt from a large chamber could also separate from it and produce small individual intrusions of gabbroids among serpentinites, as was determined in MAR at 15°N [Cannat and Casey, 1995; Cannat *et al.*, 1997]. Judging from the descriptions of the rocks (gabbroids with brown hornblende, ilmenite, apatite, and zircon; trondhjemites), these gabbroids should affiliate to the series considered in this publication. Analogous rocks (Fe-Ti-oxide hornblende gabbro and gabbronorite; our unpublished data) were dredged from the axial zone of MAR during cruise 22 of the R/V Professor Logachev, during which the Ashadze

hydrothermal field was discovered at 13°N, 44°52' W. The field contains massive sulfide mineralization among serpentinitized peridotites [Bel'tenev *et al.*, 2004]. A fairly similar situation seems to exist at other MAR hydrothermal fields with ore mineralization [Bogdanov *et al.*, 1997].

[85] **Silicic Fe-Ti-oxide series and ore-forming processes.** The solubility of fluid components, particularly water, in magmatic melts is known to decrease with decreasing pressure and, correspondingly, the solidus temperatures of the melts increase. Consequently, the ascent of hydrous melts is associated with water release from them, with this water becoming excessive under the new conditions. Upon reaching the hydrous solidus, the melts start to rapidly crystallize, and, hence, magmas of this type can only rarely reach the surface [Popov and Bogatikov, 2001]. According to experimental data, a particularly drastic decrease in the water solubility in magmatic melts occurs at pressures of approximately 1 kbar, i.e., at depths of about 3–4 km [Kadik, 1991]. This seems to be the upper limit for the ascent of most magmas of the Fe-Ti-oxide series, whose crystallization products usually occur as intrusions but are very rare in the form of lavas.

[86] The data and considerations presented above may also shed light on the genesis of mineralized fluids in the oceanic crust. The origin and development of hydrothermal systems is now thought to be related either to the circulation of waters near the surface when these waters are heated near magma chambers [Grichuk, 2000] or to the serpentinization of peridotites [Bogdanov *et al.*, 2002]. None of these

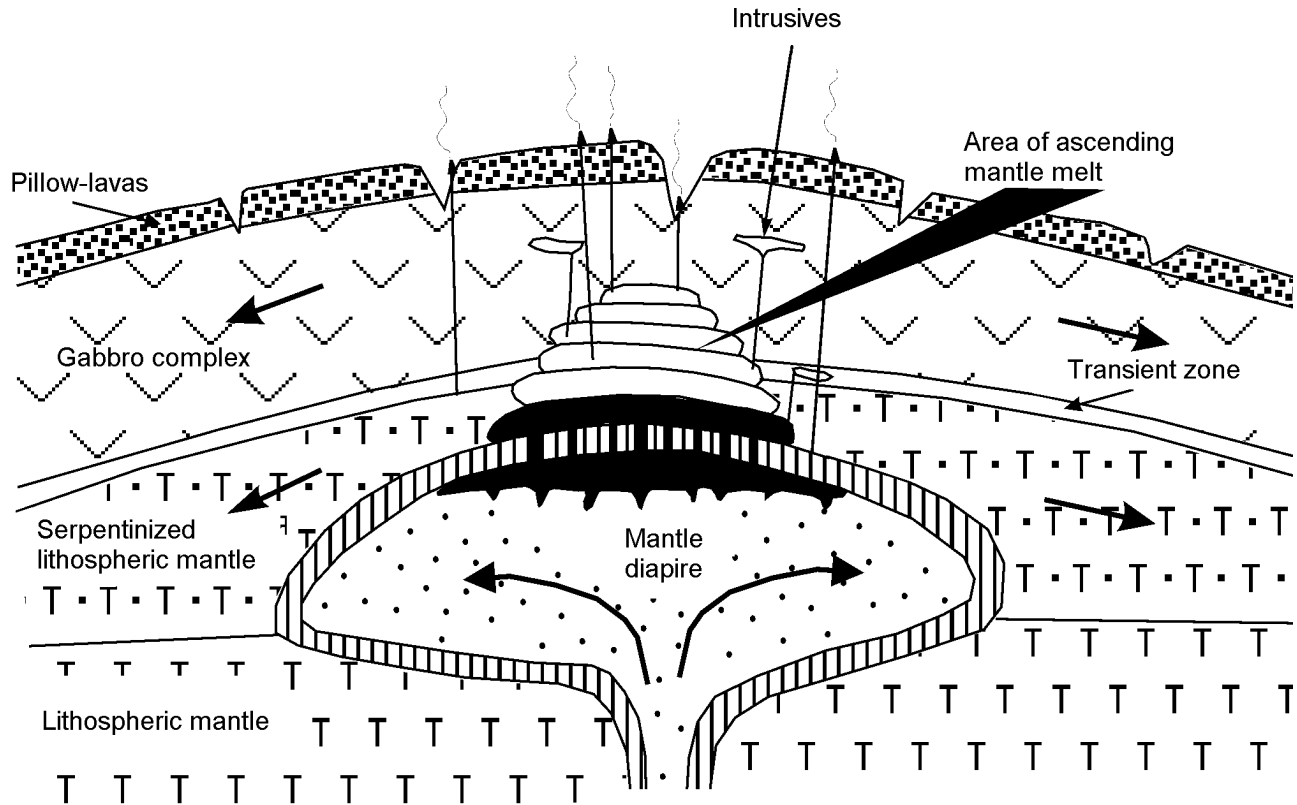


Figure 23. Hypothetical scheme for the genesis of the melts of the silicic Fe–Ti-oxide series.

models can, however, explain the occurrence of significant amounts of Pb, Zn, and Cu in these hydrothermal waters. Nevertheless, exactly these components should be contained in predominantly aqueous solution that escaped from the water-bearing melts of the silicic Fe-Ti-oxide series during decompression, and, conceivably, they also played a decisive role in the origin of ore-forming hydrothermal systems.

[87] Indeed, most sulfide occurrences in the MAR axial zone, including its black smokers, are spatially restricted to areas with rocks of the Fe-Ti-oxide association. This pertains to both the massive sulfide ores of hydrothermal-metasomatic genesis among altered gabbroids in the Markov depression [Pushcharovskii *et al.*, 2002] and the hydrothermal fields with massive sulfide mineralization in serpentinized peridotites, such as the Ashadze field in the axial MAR zone. A similar situation also seems to occur at many other mineralized hydrothermal fields in MAR [Bogdanov *et al.*, 1997].

[88] In conclusion, it is pertinent to mention that the recognition of a principally new magmatic association among the rocks of the slow-spreading MAR can be very important for understanding deep petrogenesis in similar ridges, provides insight into processes forming ore sulfide mineralization in them, and facilitates searches for black smokers and related mineral deposits on the seafloor.

Conclusions

[89] 1. The material dredged from the MAR axial zone (within the Sierra Leone MAR segment at 6°N) contains both plutonic rocks and basalts, including fresh varieties with volcanic glass crusts. The plutonic rocks belong to two associations: (i) primitive high-Mg troctolites, olivine gabbro, and gabbro, whose geochemistry is close to that of MORB, and (ii) diverse rocks with orthopyroxene, variable amounts (from 0.5 vol % to 30 vol %) of magmatic brown hornblende of the kaersutite series, ilmenite, and magnetite. The composition of these rocks ranges from ultramafic cumulates (harzburgites and lherzolites) through pyroxenites, norites, and gabbronorites to mineralized hornblende Fe-Ti-oxide gabbrodiorites and gabbrodiorites and, then, to diorites and plagiogranites (trondhjemites). Subvolcanic analogues of this association are hornblende Fe-Ti-oxide dolerites, and its volcanic analogues are basalts containing Fe-Ti oxides.

[90] 2. The rocks of the second association, which account for no less than one-third of the dredged material, were recognized as a silicic Fe-Ti-oxide magmatic series. All rocks of this series (except only the granites and diorites) are depleted in REE, Zr, Th, Ba, Hf, K, Ni, and Cu relative to

the primitive mantle and MORB and enriched in Pb, U, Ta, Nb, Zn, Cs, and Rb. This uncommon fractionation of trace elements makes this series different from the rocks of both the spreading (i.e., derivatives of MORB) and the plume (i.e., derivatives of OIB) association. The series is similar to the latter rocks only in having high contents of Ti, Ta, and Nb in the Fe-Ti-oxide gabbroids themselves, whereas most incompatible elements are deficient.

[91] 3. The parental melts of the silicic Fe-Ti-oxide association were depleted in incompatible elements, i.e., were derived from a source that had already undergone melting, and, correspondingly, these melts could not be derivatives of MORB. At the same time, they are enriched in elements usually mobilized by fluids, particularly aqueous ones, at high temperatures. This suggests that the melts were derived from water-bearing rocks. The petrological-geochemical characteristics of this series are intermediates between those of island-arc and within-plate rocks.

[92] 4. Data particularly important for understanding the genesis of the melts that produced the Fe-Ti-oxide association pertain to the plagiogranites (trondhjemites), the latest acid derivatives of this series. These rocks are characterized by high concentrations of incompatible elements, negative Eu and Sr anomalies, and are slightly enriched in LREE. According to the Nd-Sr isotopic data, the petrogenesis of these late differentiation products was participated by seawater.

[93] 5. The genesis of the parental magmas of this association is thought to have been related to the melting of the hydrated oceanic lithosphere during the emplacement of a new asthenospheric plume (protuberance on the surface of an asthenospheric lens beneath the ridge). The newly formed mantle melt passed through the upper, colder part of the plume, accumulated on its surface, and produced a large chamber, which started to ascend in compliance with the zone melting mechanism, i.e., by melting the roof rocks of the chamber and crystallizing near the bottom. The melt was thereby continuously enriched in components not only from the melting rocks of the chamber roof but also from the partly melted rocks at the peripheries of the melting zone, as well as in fluid material from the strongly heated rocks in the distant periphery. This seems to cause the unusual characteristics of the mantle-crustal melts, for example, their enrichment in SiO₂, Fe, Ti, Pb, Cu, Zn, etc.

[94] 6. Because of the large-scale assimilation of the hydrated material of the upper mantle and the lower oceanic crust and as a result of crystallization differentiation in the chamber, the composition of this melt continuously evolved, as also did the compositions of the settling crystalline phases. Hence, the ascending chamber left behind a trail in the form of a cumulate series ranging from ultramafic to mafic compositions, whose inner structure resembles that of a layered intrusion.

[95] 7. A consequence of this mechanism of the origin of the parental melts is the occurrence of inclusions of foreign minerals in the cumulus phases of the rocks, which seem to be incompletely melted fragments of the roof rocks that served as "seeds" during the crystallization of minerals in the magmatic chamber. Geochemical consequences of this mechanism are the aforementioned unusual distributions of

trace elements and REE, which can explain the genesis of the HIMU isotopic source without invoking subduction processes.

[96] 8. The hydrous melts of the silicic Fe-Ti-oxide association were characterized by limited vertical mobility because of a drastic decrease in the water solubility in melts at pressures of 1 kbar. Because of this, volcanic rocks of this association are very rare. At the same time, the solidification of the chambers of such melts at depths of 3–4 km should have been associated with the release of significant amounts of mineralized fluids enriched in Cu, Pb, Zn, and other ore components. This process is believed to be responsible for the origin of sulfide ore mineralization in the form of black smokers and massive hydrothermal-metasomatic ores, analogous to those found in the Markov depression.

[97] **Acknowledgments.** The authors thank Prof. F. Bea (Department of Mineralogy and Petrology, University of Granada, Spain) for help with the analytical part of our research. Dr. S. A. Silant'ev (Vernadsky Institute of Geochemistry and Analytical Chemistry, Russian Academy of Sciences), Dr. V. A. Simonov (Joint Institute of Geology, Geophysics, and Mineralogy, Siberian Division, Russian Academy of Sciences), and Dr. A. V. Girmis (Institute of the Geology of Ore Deposits, Petrography, Mineralogy, and Geochemistry, Russian Academy of Sciences) are thanked for looking through the manuscript and making valuable comments. This study was financially supported by the World Ocean Program of the Presidium of the Russian Academy of Sciences and Program 5 of the Earth-Science Branch of the Russian Academy of Sciences.

References

- Andersen, D. J., and D. H. Lindsley (1985), New (and final!) models for the Ti-magnetite/ilmenite geothermometer and oxygen barometer, *Eos Trans. AGU*, 66(18), 416, Spring Meeting, Abstract AGU.
- Becker, H., K. P. Jochum, and R. W. Carlson (2000), Trace element fractionation during dehydration of eclogites from high-pressure terranes and the implications for element fluxes in subduction zones, *Chem. Geol.*, 163(1–4), 65.
- Bel'tenev, V., V. Ivanov, S. Skolotnev, A. Neshcheretov, I. Rozhdestvenskaya, V. Shilov, T. Stepanova, I. Andreeva, and M. Davydov (2004), New data on ore sulfide occurrences in the Markov rift depression in the Mid-Atlantic Ridge, Equatorial Atlantic, 6°N, *Dokl. Akad. Nauk*, 395(2), 215.
- Benoit, M., G. Ceuleneer, and M. Polve (1999), The remelting of hydrothermally altered peridotite at mid-ocean ridges by intruding mantle diapirs, *Nature*, 402, 514.
- Blundy, J. D., and T. J. B. Holland (1990), Calcic equilibria and a new amphibole-plagioclase geothermometer, *Contrib. Mineral. Petrol.*, 104, 208.
- Bogatikov, O. A. (1966), *Petrology and Metallogeny of Gabbro-Syenite Complexes of the Altai-Sayan Area* (in Russian), 240 pp., Nauka, Moscow.
- Bogdanov, Yu. A., N. S. Bortnikov, and A. P. Lisitsyn (1997), Typical features in the genesis of hydrothermal sulfide deposits in the MAR axial zone, *Geol. Rudn. Mestor.*, 39(5), 409.
- Bogdanov, Yu. A., N. S. Bortnikov, and I. V. Vikent'ev (2002), Mineralogy and geochemistry of hydrothermal sulfide ores and fluid from the serpentinite-related Rainbow field, Mid-Atlantic Ridge, 36°41' N, *Geol. Rudn. Mestor.*, 44(6), 510.

- Cannat, M., and J. F. Casey (1995), An ultramafic lift in the Mid-Atlantic Ridge: Successive stages of magmatism in serpentinized peridotites from the 15°N Region, in *Mantle and Lower Crust Exposed in Oceanic Ridges and in Ophiolites*, edited by R. L. M. Vissers and A. Nicolas, p. 5, Kluwer Ac. Publ., Netherlands.
- Cannat, M., Y. Lagabriele, and H. Bougault (1992), Serpentinized peridotites and gabbros in the Mid-Atlantic Ridge Axial valley at 15°37' N and 16°52' N, *Earth Planet. Sci. Lett.*, 109, 193.
- Cannat, M., Y. Lagabriele, H. Bougault, J. Casey, N. de Coutures, L. Dmitriev, and Y. Fouquet (1997), Ultramafic and gabbroic exposures at the Mid-Atlantic Ridge: geological mapping in the 15° region, *Tectonophysics*, 279(1-4), 193.
- Dick, H. J. B., P. S. Meyer, and S. H. Bloomer (1991), Lithostratigraphic evolution of an in situ section of oceanic layer 3, in *Proc. ODP, Sci. Results, 118: College Station, TX (Ocean Drilling Program)*, edited by R. P. Von Herzen, P. T. Robinson, p. 439, Texas A&M University, Texas.
- Dick, H. J. B., J. H. Natland, and J. W. Alt (2000), A long in situ section of the lower oceanic crust: results of ODP Leg 176 drilling at the Southwest Indian Ridge, *Earth Planet. Sci. Lett.*, 179, 31.
- Dick, H. J. B., P. T. Robinson, and P. S. Meyers (1992), The plutonic foundation of a low-spreading ridge, *Am. Geophys. Union Monograph*, 70, 1.
- Dmitriev, L. V., S. Yu. Sokolov, V. G. Melson, and T. O'Hirn (1999), Plume-related spreading association of basalts and their reflection in the petrological and geochemical characteristics of the northern part of the Mid-Atlantic Ridge, *Russian J. Earth. Sci.*, 1(6), 457.
- Douglass, J., J.-G. Schilling, and D. Fontignie (1999), Plume-ridge interactions in the Discovery and Shona mantle plumes with the southern Mid-Atlantic Ridge (40°-55°S), *J. Geophys. Res.*, 104(B2), 2941.
- Fershtater, G. B., V. V. Kholodnov, and V. S. Borodina (2001), Formation conditions and genesis of Riphean ilmenite-titanomagnetite deposits in the Urals, *Geol. Ore Deposits*, 43(2), 112.
- Fowler, C. M. R. (2004), *The Solid Earth, An Introduction to Global Geophysics*, 500 pp., Cambridge Univ. Press, New York.
- Gaetani, G. A., and T. L. Grove (1998), The influence of water on the melting of mantle peridotite, *Contrib. Miner. Petrol.*, 131, 323.
- Grichuk, D. V. (2000), *Geodynamic Models for Submarine Hydrothermal Systems* (in Russian), 303 pp., Nauchnyi Mir, Moscow.
- Hannigan, R. E., A. R. Basu, and F. Teichmann (2001), Mantle reservoir geochemistry from statistical analysis of ICP-MS trace element data of equatorial Mid-Atlantic MORB glasses, *Chem. Geol.*, 175(3-4), 397.
- Holm, P. M. (2002), Sr, Nd and Pb isotopic composition of in situ lower crust at the Southwest Indian Ridge: results from ODP Leg 176, *Chem. Geol.*, 184(3-4), 195.
- Kadik, A. A., (Ed.) (1991), *Fluids and Redox Reactions in Magmatic Systems*, 256 pp., Nauka, Moscow.
- Kushiro, I. (1969), The system forsterite-diopside-silica with and without water at high pressure, *Am. J. Sci.*, 207a, 269.
- Kushiro, I., Y. Syono, and S. Akimoto (1968), Melting of a peridotite nodule at high pressures and high water pressures, *J. Geophys. Res.*, 73, 6023.
- Laz'ko, E. E., and E. V. Sharkov, (Eds.), (1988), *Magmatic Rocks*, vol. 5, *Ultramafic Rocks*, 502 pp., Nauka, Moscow.
- Lombardo, B., D. Rubatto, and D. Castelli (2002), Ion microprobe U-Pb dating of zircon from a Monviso metaplagiogranite: Implications for the evolution of the Piedmont-Liguria Tethys in the Western Alps, *Ophioliti*, 27(2), 109.
- McDonough, W. F., and S.-S. Sun (1995), The composition of the Earth, *Chem. Geol.*, 120, 223.
- Natland, J. H., P. S. Meyer, H. J. B. Dick, and S. H. Bloomer (1991), Magmatic oxides and sulfides in gabbroic rocks from Hole 735B and later development of the liquid line of descent, in *Proc. ODP, Sci. Results, 118, College Station, TX (Ocean Drilling Program)*, edited by R. P. Von Herzen, P. T. Robinson, p. 75, Texas A&M University, Texas.
- Ozawa, K., P. S. Meyer, and S. H. Bloomer (1991), Mineralogy and textures of iron-titanium oxide gabbros and associated olivine gabbro from Hole 735B, in *Proc. ODP, Sci. Results, 118, College Station, TX (Ocean Drilling Program)*, edited by R. P. Von Herzen, P. T. Robinson, p. 41, Texas A&M University, Texas.
- Peacock, S. M., T. Rushmer, and A. B. Thompson (1994), Partial melting of subducting oceanic crust, *Earth Planet. Sci. Lett.*, 121, 227.
- Pearce, J. A. (2002), The oceanic lithosphere, *JOIDES Journal*, Spec. issue, 28(1), 61.
- Piccardo, G. B., O. Muntener, and A. Zanetti (2004), The Lanzo peridotite: melt/peridotite interaction in the mantle lithosphere of the Jurassic Ligurian Tethys, *Ophioliti*, 29(1), 37.
- Pilot, J., C.-D. Werner, F. Haubrich, and N. Baumann (1998), Palaeozoic and Proterozoic zircons from Mid-Atlantic Ridge, *Nature*, 393(6686), 676.
- Popov, V. S., and O. A. Bogatikov, (Eds.), (2001), *Petrography and Petrology of Magmatic, Metamorphic, and Metasomatic Rocks*, 766 pp., Logos, Moscow.
- Powell, R., and M. Powell (1977), Geothermometry and oxygen barometry using coexisting iron-titanium oxides: a reappraisal, *Mineral. Mag.*, 41(318), 257.
- Pushcharovskii, Yu. M. (2001), *Fundamental Problems of General Tectonics*, 174 pp., Nauchnyi Mir, Moscow.
- Pushcharovskii, Yu., N. Bortnikov, S. Skolotnev, A. Peive, V. Kolobov, N. Tsukanov, S. Lyapunov, E. Sharkov, and M. Stolyarov (2002), Massive and stringer-disseminated sulfide mineralization in the Mid-Atlantic Ridge near the Sierra Leone Fracture Zone in relation to its geologic structure, *Dokl. Akad. Nauk*, 384(1), 83.
- Reverdatto, V. V., A. Yu. Selyatitsky, D. N. Remizov, and V. V. Khlestov (2005), Geochemical distinctions between "mantle" and "crustal" high/ultrahigh-pressure peridotites and pyroxenites, *Dokl. Ross. Akad. Nauk* (in Russian), 400(1), 72.
- Ross, K., and D. Elthon (1996), Cumulates from strongly depleted mid-ocean-ridge basalt, *Nature*, 365, 826.
- Rubatto, D., and D. Gebauer (2000), Use of cathodeluminescence for U-Pb zircon dating by ion microprobe: some examples from the Western Alps, in *Cathodeluminescence in Geosciences*, edited by M. Pagel, V. Barbin, P. Blank, and D. Ohnenstetter, p. 375, Springer, Berlin.
- Rudnick, R. (1990), Growing from below, *Nature*, 347(6295), 711.
- Ryabchikov, I. D. (2003), Mechanism and conditions of magma formation in mantle plumes, *Petrology*, 11(6), 496.
- Sandwell, D. T., and W. H. Smith (1997), Marine gravity anomaly from Geosat and ERS-1 satellite altimetry, *J. Geophys. Res.*, 102, 10,039.
- Schiano, P., R. Clocchiatti, J.-P. Lorand, D. Massare, E. Deloule, and M. Chaussidon (1997), Primitive basaltic melts included in podiform chromites from the Oman ophiolite, *Earth Planet. Sci. Lett.*, 146(3-4), 489.
- Schiano, P., R. Clocchiatti, N. Shimizu, R. C. Maury, K. P. Jochum, and A. W. Hofmann (1995), Hydrous, silica-rich melts in the sub-arc mantle and their relationship with erupted arc lavas, *Nature*, 377(6550), 591.
- Schilling, J.-G., B. B. Hanan, B. McCully, and R. H. Kingsley (1994), Influence of the Sierra Leone mantle plume on the equatorial MAR: a Nd-Sr-Pb isotopic study, *J. Geophys. Res.*, 99, 12005.
- Schilling, J.-G., M. Zajac, R. Evans, T. Johnston, W. White, J. D. Devine, and R. Kingsley (1983), Petrologic and geochemical variations along the Mid-Atlantic Ridge from 29°N to 73°N, *Am. J. Sci.*, 283(6), 510.
- Sharkov, E. V. (1980), *Petrology of Layered Intrusions*, 184 pp., Nauka, Leningrad.
- Sharkov, E. V. (2003a), Layered intrusions as transitional magma chambers above the local plumes of large igneous rock provinces: evidence from the Early Paleoproterozoic province

- of a siliceous highly magnesian rock series in the Baltic Shield, *Russian J. Earth Sci.*, 5(4), 324.
- Sharkov, E. V. (2003b), Where and why does the ancient continental crust disappear?—Systems of volcanic arcs and backarc basins, in *Problems of Global Geodynamics, Theoretical Seminar at OGGGN Ros. Akad. Nauk in 1999–2001*, edited by D. V. Rundkvist, issue 2, p. 276, OGGGN Ros. Akad. Nauk, Moscow.
- Sharkov, E. V., N. S. Bortnikov, and O. A. Bogatnikov (2004a), Mesozoic zircon in gabbroanorthites from the Markov depression, MAR axial zone at 6°N, *Dokl. Ross. Akad. Nauk*, 396(5), 675.
- Sharkov, E. V., K. N. Shatagin, and I. V. Chernyshev (2004b), Sr-Nd heterogeneity of magmatic and metasomatic rocks in the MAR axial zone at 6°N, paper presented at XVII Symp. of Isotopic Geochemistry, Vernadsky Institute of Geochemistry and Analytical Chemistry, Russ. Acad. Sci., Moscow.
- Sharkov, E. V., A. V. Chistyakov, and E. E. Laz'ko (2001), Structure of the layered complex of the Voikar ophiolitic association, Polar Urals as an indicator of mantle processes beneath the backarc sea, *Geokhimiya*, 9, 915.
- Sharkov, E. V., V. V. Liachovich, and G. V. Ledneva (1994), Petrology of the Early Proterozoic Drusite complex, White Sea Region, with reference to the Pezhostrov massif, North Karelia, *Petrology*, 2(5), 454.
- Sharkov, E. V., V. F. Smolkin, and I. S. Krassivskaya (1997), Early Proterozoic magmatic provinces of high-Mg boninite-like rocks in the eastern Baltic Shield, *Petrologiya*, 5(5), 503.
- Silantyev, S. A. (1998), Formation conditions of the plutonic complex in the Mid-Atlantic Ridge, 13°–17°N, *Petrologiya*, 6(4), 381.
- Silantyev, S. A., B. A. Bazylev, and L. V. Dmitriev (2002), Relations between plume magmatism and mantle metasomatism beneath the Mid-Atlantic Ridge, Int. Symp. on Mantle Plumes and Magmatism, p. 219, Probel-2000, Moscow-Petrozavodsk.
- Simonov, V. A., V. Yu. Kolobov, and A. A. Peive (1999), *Petrology and Geochemistry of Geodynamic Processes in the Central Atlantic* (in Russian), 226 pp., SO RAN, NITs OIGGM, Novosibirsk.
- Skolotnev, S. G., A. A. Peyve, N. S. Bortnikov, G. N. Savel'eva, V. A. Simonov, E. V. Sharkov, N. V. Tsukanov, I. N. Turko, and T. A. Demidova (2003a), Geology of ore-hosting rift depressions near the Sierra Leone Fracture Zone in the equatorial Atlantic, *Dokl. Ross. Akad. Nauk*, 391(2), 232.
- Skolotnev, S. G., A. A. Peyve, S. M. Lyapunov, V. A. Simonov, Yu. E. Glazyrin, and V. Yu. Kolobov (2003b), MAR volcanism in the Sierra Leone Fracture Zone region, Central Atlantic, *Russian J. Earth Sci.*, 5(2), 232. available at: <http://rjes.wdcb.ru/v05/tje03117/tje03117.htm>
- Sobolev, A. V., L. V. Danyushevskii, L. V. Dmitriev, and N. M. Sushchevskaya (1988), High-Al magnesian tholeiite as one of the parental melts of MORB, *Geokhimiya*, 10, 1522.
- Spenser, K. J., and D. H. Lindsley (1981), A solution model for coexisting iron-titanium oxides, *Am. Mineral.*, 66(11–12), 1189.
- Sun, S.-S., and W. F. McDonough (1989), Chemical and isotope systematics of oceanic basalts: implication for mantle composition and processes, in *Magmatism in the oceanic basins*, *Geol. Soc. Spec. Publ.*, vol. 42, edited by A. D. Sanders, M. J. Norry, p. 313, "London", London.
- Tatsumi, Y., D. L. Hamilton, and R. W. Nesbitt (1986), Chemical characteristic of the fluid phase released from subducted lithosphere and origin of arc magmas: evidence from high pressure experiments and natural rocks, *J. Volcanol. Geotherm. Res.*, 29(1–4), 293.
- Tenthorey, E., and J. Jermann (2004), Composition of fluids during serpentine breakdown in subduction zones: evidence for limited boron mobility, *Geology*, 32(10), 865.
- Wager, L. R., and G. M. Brown (1968), *Layered Igneous Rocks*, Freeman, San Francisco.
- Watson, B. E., and T. M. Harrison (1983), Zircon saturation revisited: temperature and compositional effects in variety of crustal magma types, *Earth Planet. Sci. Lett.*, 64, 295.
- Wilson, M. (1989), *Igneous petrogenesis, A global approach*, 466 pp., Unwin Human, London.
- Zindler, A., and S. R. Hart (1986), Chemical Geodynamics. mantle chemical heterogeneity: a matter of scale, *Annu. Rev. Earth Planet. Sci.*, 14, 493.
- Zinger, T. F., and B. V. Belyatsky (2001), Cathodoluminescence in Geosciences: new insights from CL in combination with other techniques, in *abstracts Germany*, p. 136, Freiberg University of Mining and Technology, Freiberg, TU Bergakademie, September 6–8.

N. S. Bortnikov, A. V. Chistyakov, E. V. Sharkov, Institute of the Geology of Ore Deposits, Petrography, Mineralogy, and Geochemistry (IGEM), Russian Academy of Sciences, 35 Staromonetnyi per., Moscow, 109017 Russia

T. F. Zinger, Institute of Precambrian Geology and Geochronology, Russian Academy of Sciences, 2 nab. Makarova, St. Petersburg, 199034 Russia